ELEMENTA
Science of the Anthropocene

Jacques, C, et al. 2021. Sources and sinks of methane in sea ice: Insights from stable isotopes. *Elem Sci Anth*, 9: 1. DOI: https://doi.org/10.1525/elementa.2020.00167

RESEARCH ARTICLE

Sources and sinks of methane in sea ice: Insights from stable isotopes

Caroline Jacques[1], Célia J. Sapart[1,2], François Fripiat[1], Gauthier Carnat[1], Jiayun Zhou[1,3], Bruno Delille[3], Thomas Röckmann[2], Carina van der Veen[2], Helge Niemann[4,5,6], Tim Haskell[7], and Jean-Louis Tison[1,*]

We report on methane (CH_4) stable isotope ($\delta^{13}C$ and δ^2H) measurements from landfast sea ice collected near Barrow (Utqiagvik, Alaska) and Cape Evans (Antarctica) over the winter-to-spring transition. These measurements provide novel insights into pathways of CH_4 production and consumption in sea ice. We found substantial differences between the two sites. Sea ice overlying the shallow shelf of Barrow was supersaturated in CH_4 with a clear microbial origin, most likely from methanogenesis in the sediments. We estimated that in situ CH_4 oxidation consumed a substantial fraction of the CH_4 being supplied to the sea ice, partly explaining the large range of isotopic values observed ($\delta^{13}C$ between –68.5 and –48.5 ‰ and δ^2H between –246 and –104 ‰). Sea ice at Cape Evans was also supersaturated in CH_4 but with surprisingly high $\delta^{13}C$ values (between –46.9 and –13.0 ‰), whereas δ^2H values (between –313 and –113 ‰) were in the range of those observed at Barrow. These are the first measurements of CH_4 isotopic composition in Antarctic sea ice. Our data set suggests a potential combination of a hydrothermal source, in the vicinity of the Mount Erebus, with aerobic CH_4 formation in sea ice, although the metabolic pathway for the latter still needs to be elucidated. Our observations show that sea ice needs to be considered as an active biogeochemical interface, contributing to CH_4 production and consumption, which disputes the standing paradigm that sea ice is an inert barrier passively accumulating CH_4 at the ocean-atmosphere boundary.

Keywords: Methane, Stable isotopes, Sea ice, Arctic, Antarctic, Production and consumption pathways

1. Introduction

The contribution of oceans to the atmospheric methane (CH_4) budget is subject to large uncertainties given the small coverage of existing dissolved CH_4 measurements and the poor understanding of the processes at play. Unraveling the mechanisms involved in CH_4 emission (removal) from (in) the ocean is important to understanding the major ongoing change in the CH_4 global budget: a renewed increase in atmospheric CH_4 growth rates after a period of stabilization between 1999 and 2006 (Nisbet et al., 2016). Understanding these mechanisms is especially relevant for the Arctic Ocean, as massive reservoirs of CH_4 have been reported in the seafloor, mainly in the subsea permafrost and in gas hydrates, which are both highly sensitive to temperature changes (O'Connor et al., 2010; Schuur et al., 2015; Dean et al., 2018; Ferré et al., 2020). In the context of climate change, the contribution of the Arctic Ocean to CH_4 emissions is expected to increase, particularly in shallow shelf areas, where sedimentary CH_4 can directly escape to the atmosphere (Shakhova et al., 2010a; Shakhova et al., 2010b; Sapart et al., 2017).

In polar regions, CH_4 fluxes between the ocean and the atmosphere are further influenced by sea ice. In most of the ocean biogeochemical models, sea ice is still seen as an inert barrier, preventing gas exchange between seawater and the atmosphere (e.g., Aumont et al., 2015). However, observations during the recent decades suggest that sea ice is an active biogeochemical interface at the ocean–atmosphere boundary, contributing up to 60% of the primary production in some parts of the Arctic Ocean (Fernández-Méndez et al., 2015) and 50% of the CO_2 uptake south of 50°S (Delille et al., 2014). The impact of sea ice on

[1] Laboratoire de Glaciologie, Université libre de Bruxelles, Bruxelles, Belgium

[2] Institute for Marine and Atmospheric research Utrecht (IMAU), Utrecht University, Utrecht, the Netherlands

[3] Unité d'Océanographie Chimique, Université de Liège, Liège, Belgium

[4] Department of Marine Microbiology and Biogeochemistry, Royal Netherlands Institute for Sea Research (NIOZ), Texel, the Netherlands

[5] Department of Earth Sciences, Faculty of Geosciences, Utrecht University, Utrecht, the Netherlands

[6] CAGE—Centre for Arctic Gas Hydrate, Environment and Climate, Department of Geosciences, UiT The Arctic University of Norway, Tromsø, Norway

[7] Callaghan Innovation, Wellington, New Zealand

* Corresponding author:
Email: jean-louis.tison@ulb.be

the exchange of CH_4 between the ocean and the atmosphere is still largely unknown, as well as the potential for CH_4 production and consumption within the sea ice itself. Damm et al. (2015) observed a large CH_4 supersaturation in sea-ice brine channels and suggested that sea ice might favor methanogenesis. Brine discharge from sea ice during cold months would then enrich the underlying seawater in CH_4, which could be released under a fractional sea-ice cover, mainly in autumn, when turbulence breaks the haline stratification, allowing CH_4 efflux to the atmosphere (Damm et al., 2015). Significant CH_4 elevations were measured in the Arctic atmospheric boundary layer, associated with fractional sea-ice cover, although the underlying process was not identified (Kort et al., 2012). In contrast, He et al. (2013) reported negative air–ice CH_4 fluxes in summer. Due to the lack of measurements and heterogeneity of the system, these fluxes to date are poorly characterized and quantified, so that the role of sea ice as a net sink or source of CH_4 remains unclear.

Studying the stable isotopic composition of CH_4 provides useful information on production and consumption processes, as these induce characteristic isotopic fractionations. In aquatic environments, CH_4 production is thought to occur primarily under strictly anaerobic conditions in the sediments, either via thermogenic degradation of organic matter (associated with high $\delta^{13}C$ signatures ranging between −50 and −20 ‰, and δ^2H signatures ranging between −275 and −100 ‰) or via microbial production (associated with comparatively low $\delta^{13}C$ signatures between −110 and −50 ‰, and δ^2H signatures ranging between −400 and −150 ‰; Whiticar, 1999). However, the ubiquitous CH_4 excess in oceanic surface waters despite the presence of oxygen, referred to as the "marine methane paradox," challenges this view (Kiene, 1991; Tilbrook and Karl, 1995; Reeburgh, 2007; Karl et al., 2008; Bižić et al., 2020). The few measurements of $\delta^{13}C$ signatures associated with this excess CH_4 at the ocean surface show values between −47 and −44 ‰ (Holmes et al., 2000; Sasakawa et al., 2008), which is slightly enriched in ^{13}C compared to the atmospheric value. Damm et al. (2010) report $\delta^{13}C$ signatures ranging between −46 and −38 ‰ in the top 150 m of the water column in the central Arctic Ocean. New aerobic pathways have hence been proposed to resolve this paradox (**Table 1**), such as CH_4 production from methylated compounds in oligotrophic oceanic waters (Karl et al., 2008; Damm et al., 2010), bacterial degradation of organic matter phosphonates (Karl et al., 2008; Repeta et al., 2016), inorganic carbon fixation by cyanobacteria and marine algae (Lenhart et al., 2016; Klintzsch et al., 2019; Bižić et al., 2020), and methylated sulphur precursors by marine algae (Lenhart et al., 2016; Klintzsch et al., 2019). Recently, incubations of samples from Lake Stechlin (Germany) showed that phytoplankton produced CH_4 under oxic conditions, with diatoms and cyanobacteria producing CH_4 more enriched in ^{13}C than atmospheric CH_4 (Hartmann et al., 2020). The influence of these aerobic pathways on the CH_4 isotopic budget remains elusive. The isotopic composition of CH_4 trapped in sea ice was measured in only 3 studies, with $\delta^{13}C$ values ranging between −83 and −36 ‰ (Lorenson and Kvenvolden, 1995; Damm et al., 2015; Uhlig et al., 2018). The processes leading to the wide range of $\delta^{13}C$ signatures observed in sea ice clearly require further investigation and δ^2H signatures remain to be measured.

In this study, we report the CH_4 stable isotopic composition (both $\delta^{13}C$ and δ^2H) in landfast sea ice from the Arctic (Barrow, now Utqiagvik, Alaska) and the Southern Ocean (Cape Evans, Ross Sea). At both locations, 3 sea-ice cores were sampled across the winter–spring transition, which gave us a unique opportunity to investigate the relevant CH_4 sources and the seasonal variation of the isotopic composition of CH_4 in sea ice.

2. Study location

We analyzed the CH_4 stable isotope composition in 3 sea-ice cores from the Arctic Ocean, collected on April 3, May 8, and June 5, in the framework of a survey conducted between January and June 2009 on landfast sea ice near Barrow (Utqiagvik, Alaska; **Figure 1A**). The study site, together with the physicochemical properties of these ice cores, has been described in detail by Zhou et al. (2013). Of particular relevance here is that the water depth between the sediments (underlain by subsea permafrost; Shakhova et al., 2010a) and the ice cover was about 6.5 m. Ice cores were collected using an electromechanical drilling system and immediately packed in plastic bags, stored in insulated boxes equipped with cooling bags to limit potential brine and gas losses from the ice, and then transported at −25°C to our laboratory as described in Zhou et al. (2013).

We also analyzed CH_4 concentration and stable isotope composition in 3 cores from the Antarctic coast, sampled on September 19 and November 7 and 30, 2012, on landfast sea ice at Cape Evans in the Ross Sea, in the framework of the project Year Round survey of Ocean-Sea Ice-Air Exchanges in Antarctica (YROSIAE; **Figure 1B**). The water column depth at the sampling site was approximately 86 m. Noteworthy features of the study site include its location near the flanks of an active volcano, Mount Erebus, and in the vicinity of the Ross Ice Shelf. A thorough description of the study site, the sampling procedure, and sea-ice physicochemical properties can be found in Carnat et al. (2014) and Van der Linden et al. (2020).

3. Methods

3.1. CH_4 concentration measurement

At both locations, CH_4 was extracted from bulk ice at a 5-cm resolution using the melting–refreezing method developed by Raynaud et al. (1983). The extracted CH_4 was then separated from the gas mixture by gas chromatography and analyzed with a Flame Ionisation Detector, as described for the work at Barrow in Zhou et al. (2014). The typical standard deviation of the CH_4 concentration measurement derived from Barrow sea-ice sample triplicates was $\pm$ 1.1 nM. This estimate was not available for the Cape Evans samples given the limited amount of ice available.

As only half an ice core collected on May 8 in Barrow was available for both CH_4 concentration and isotope analyses, CH_4 concentrations for this specific core were inferred from the $\delta^{13}C$ measurements. This method assumes that 100% of the CH_4 trapped in the ice sample

Table 1. Alternative methane (CH_4) production pathways in aerobic surface waters. DOI: https://doi.org/10.1525/elementa.2020.00167.t1

Pathway	Organisms	Environment	CH_4 Substrate	Comment	Study
Methylotrophic methanogenesis	Archaea	Anaerobic microniches in oxic surface waters of Storfjorden	Dimethylsulfoniopropionate (DMSP)	CH_4 production associated with summer phytoplankton bloom	Damm et al. (2008)
By-product of autotrophic C fixation	Phytoplankton (*Emiliania huxleyi*)	Lab incubations, oxic conditions	Bicarbonate	No comment	Lenhart et al. (2016)
By-product of autotrophic protein and DMSP synthesis	Phytoplankton (*E. huxleyi*)	Lab incubations, oxic conditions	Methionine	No comment	Lenhart et al. (2016)
C–P lyase phosphonate degradation pathway	Bacteria	Seawater and pure culture incubations, oxic conditions	Methyl phosphonate esters (dissolved organic matter)	No comment	Karl et al. (2008) and Repeta et al. (2016)
CH_4 formation from thioethers (methionine and dimethyl sulfide [DMS]) and their corresponding sulfoxides (methyl sulfoxide [MSO] and dimethyl sulfoxide [DMSO]) catalyzed by nonheme iron-oxo (IV)	Phytoplankton (*E. huxleyi*, *Phaeocystis globosa* and *Chrysochromulina sp.*)	Lab incubations, oxic conditions	DMS, DMSO, and MSO	Response to oxidative stress	Klintzsch et al. (2019)
Photosynthesis by-product	Cyanobacteria	Lab incubations, oxic conditions	Sodium hydrogen carbonate ($NaHCO_3$)	No comment	Bižić et al. (2020)
By-product of autotrophic C fixation (precise pathway to be investigated further)	Cyanobacteria, diatoms, green algae, and cryptophytes	Lab incubations, oxic conditions	No substrate	Diatoms and cyanobacteria tend to produce CH_4 more enriched in ^{13}C than atmospheric CH_4	Hartmann et al. (2020)
			$NaHCO_3$	All investigated organisms produce CH_4	

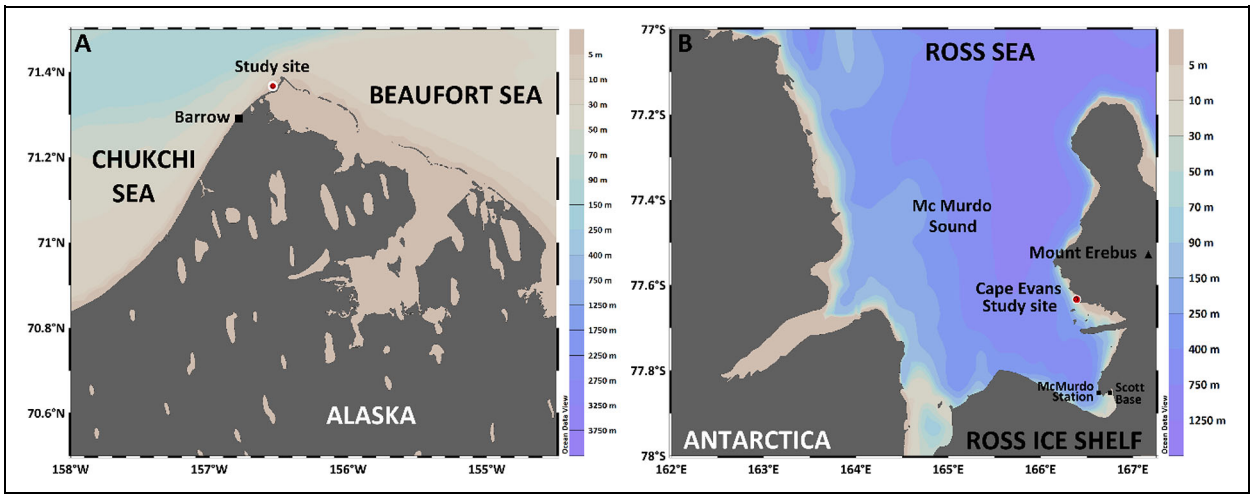

Figure 1. Study sites for sea-ice core sampling. (A) Barrow (Utqiagvik), Chukchi Sea (Arctic), and (B) Cape Evans, Ross Sea (Antarctic). DOI: https://doi.org/10.1525/elementa.2020.00167.f1

is extracted for isotopic measurements, although the extraction efficiency was estimated to >97% in Sapart et al. (2011). The determination of the concentration used a calibration curve where increasing volumes of reference air with a known mixing ratio were injected into the isotope ratio mass spectrometer (IRMS), which allowed to derive the number of moles of CH_4 in an unknown sample from the peak area. The amount was then converted to concentration, accounting for the mass of ice used for the measurement. To estimate the error associated with this method, we also analyzed samples from cores that had been characterized previously by GC (stations on April 3 and June 5). The comparison showed a good agreement and the mean standard deviation of the concentrations obtained with those two methods was $\pm$1.5 nM.

As most of the CH_4 is expected to be in the brines, we also calculated the CH_4 concentration in brine by dividing the CH_4 concentration measured in bulk ice by the brine volume fraction (following Cox and Weeks, 1983).

According to Golden et al. (1998), columnar sea ice with a brine volume fraction <5% can be considered impermeable to liquid transport. For gases, an empirical threshold of 7%–8% has been proposed (Zhou et al., 2013). In this study, we consider that sea ice with a brine volume fraction between 5% and 8% is at the permeability threshold and that sea ice with a brine volume fraction above 8% is permeable.

3.2. Stable isotopic composition of CH_4

Stable isotope analyses were conducted in 3 steps: first, extraction of the gas trapped within sea-ice samples with a dry extraction method (Sapart et al., 2011); second, the preconcentration and cryofocusing of CH_4; and third, its injection via an open split system to a ThermoFinnigan Delta^{plus} XL IRMS to measure alternatively $\delta^{13}C$ and δ^2H signatures (Brass and Röckmann, 2010; Sapart et al., 2017; Jacques et al., 2020). Stable isotope measurements were normalized using a one-point calibration, with a reference gas characterized by a $\delta^{13}C$–CH_4 value of –47.8 ‰ versus Vienna Pee Dee Belemnite (VPDB) and a δ^2H–CH_4 value of –83.4 ‰ versus Vienna Standard Mean Ocean Water (VSMOW). Such an approach may lead to scale compression effects, but the isotope scale is checked regularly at the Utrecht University laboratory, using high volume samples collected from polar firn (Sapart et al., 2013). Stable isotope values were corrected to account for daily variability and nonlinearity effects of the system and reported relative to international standards in ‰ versus VPDB for $\delta^{13}C$ values and ‰ versus VSMOW for δ^2H values:

$$\delta^{13}C(‰) = \left(\frac{^{13}C/\,^{12}C_{sample}}{^{13}C/\,^{12}C_{VPDB}} - 1 \right) \times 1,000\,, \quad (1)$$

$$\delta^{2}H(‰) = \left(\frac{^{2}H/\,^{1}H_{sample}}{^{2}H/\,^{1}H_{VSMOW}} - 1 \right) \times 1,000\,. \quad (2)$$

The reproducibility for $\delta^{13}C$ and δ^2H measurements, calculated from the standard deviation on several reference air injections over the period of measurements reported here, was 0.4 ‰ and <5 ‰, respectively. The cores dedicated to stable isotope analyses were cut to obtain a minimum of 500 g of ice per sample to provide sufficient CH_4 for a precise IRMS measurement. This approach implies a lower sample resolution than for the concentration analyses, and also differences between $\delta^{13}C$ and δ^2H measurements, depending on the amount of ice available, and that the isotopic sample resolution does not match the 5-cm resolution of the concentration analyses. We therefore averaged CH_4 concentrations to obtain one concentration value per isotopic measurement.

In this article, we have estimated the isotopic fractionation ε (degree of isotopic discrimination of the two isotopes ^{13}C and ^{12}C or ^2H and ^1H as they are converted from reactants to product) during the potential oxidation process, using our data sets and the approximation from Mariotti et al. (1981):

$$\delta CH_4 = \delta CH_{4\,init} + \varepsilon \ln f, \quad (3)$$

where δCH_4 is the isotopic value of the remaining CH_4 fraction, $\delta CH_{4\ init}$ is the initial CH_4 isotopic value, and "f" is the remaining CH_4 fraction.

Because, in the process of CH_4 oxidation, the residual CH_4 fraction is steadily enriched in heavy isotopes as CH_4 is consumed, the slope of the observed relationship is negative.

The isotopic fractionation ε (expressed in ‰) is here defined as:

$$\varepsilon(‰) = (\alpha - 1)\, x1,000, \tag{4}$$

where α, the fractionation factor, is taken as:

$$\alpha = \frac{^{13}k}{^{12}k}, \tag{5}$$

where "^{n}k" is the rate constant for the ^{n}C-reactant (CH_4).

In this way, we report (more intuitive) positive isotopic fractionation ε in the residual CH_4 fraction for an expression of the fractionation factor similar to the one used in several other studies (Mariotti et al., 1981; Whiticar, 1999).

We are aware of the potential limitations of the Mariotti et al. (1981) approximation, especially for hydrogen (Hayes, 2004), but are comfortable with the use of it, given the range of observed isotopic values for both $\delta^{13}C$ and $\delta^{2}H$.

4. Modeling

To investigate the CH_4 isotope systematics, we built a simple one-box model (**Figure 2**). Our model does not address the full complexity of the sea-ice system but helps in assessing the potential contribution of four different processes to the CH_4 isotopic signature: microbial oxidation, microbial production, exchange with the atmosphere, and supply from underlying seawater. CH_4 is removed from the system by microbial oxidation, which is characterized by a typical rate (MO_x) and isotopic fractionation (ε_{MOx}). CH_4 is supplied to the system (1) by microbial production with a characteristic isotopic signature ($\delta^{13}C_{MOg}$) at a certain rate (MO_g) and/or (2) from underlying seawater, via bubbles or diffusive exchange, with a characteristic isotopic signature ($\delta^{13}C_S$) at a certain rate (S). Exchange with dissolved CH_4 in equilibrium with the atmosphere is parametrized as a mixing between observed properties (i.e., concentration and $\delta^{13}C$) and a hypothetical pool in equilibrium with the atmosphere ($[CH_4]_{eq}$ and $\delta^{13}C = -47$ ‰), using a first-order exchange rate coefficient (k). Two governing equations describe the evolution of the concentration of CH_4 and $^{13}CH_4$ with time:

$$\frac{d[CH_4]}{dt} = -MOx + S + MOg + k * \left([CH_4]_{eq} - [CH_4]\right), \tag{6}$$

$$\frac{d[^{13}CH_4]}{dt} = -MOx * \frac{[^{13}CH_4]}{[CH_4]} * (1 - \varepsilon_{MOx}) + {}^{13}S + {}^{13}MOg + k * \left([^{13}CH_4]_{eq} - [^{13}CH_4]\right). \tag{7}$$

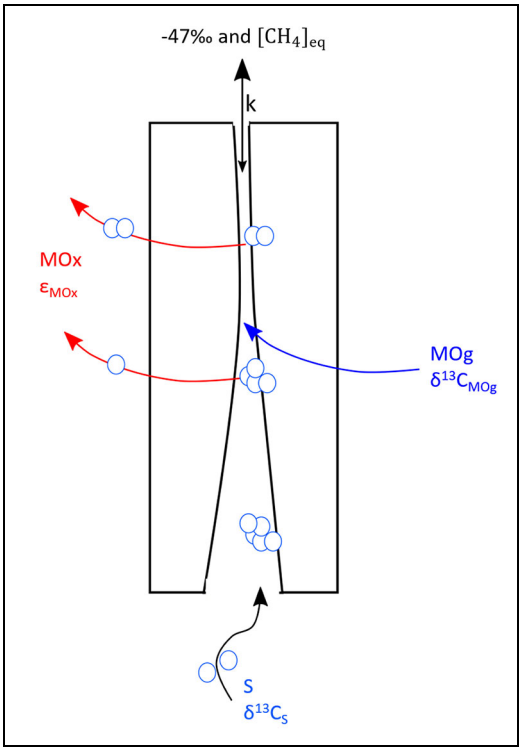

Figure 2. Conceptual representation of the one-box model used in this study. The processes considered are CH_4 oxidation rate (MO_x) and associated isotopic fractionation (ε_{MOx}), CH_4 production rate (MOg), and associated isotopic signature ($\delta^{13}C_{MOg}$), supply of CH_4 from underlying seawater as bubbles or in dissolved state (S) and associated isotopic signature ($\delta^{13}C_S$), and exchange with dissolved CH_4 in equilibrium with the atmosphere ($[CH_4]_{eq}$ and $\delta^{13}C$ of –47 ‰). DOI: https://doi.org/10.1525/elementa.2020.00167.f2

An important question is whether the CH_4 concentration in bulk ice or in brines should be used in the calculations. For mixing processes with the atmosphere involving CH_4 diffusion and/or mechanical mixing, brine concentration should be used. Indeed, solute and bubbles are well recognized as located exclusively within the brine network (Tison et al., 2017). The concentration of a solute in brines, however, is highly dependent on internal physical processes such as brine shrinking (widening) due to a temperature decrease (increase) and the vertical migration of brines in the ice cover, in response to density instabilities in permeable ice (Petrich and Eicken, 2017). To tackle processes such as closed-system microbial oxidation or production, brine concentrations cannot be used because brine concentration and dilution at a given level will affect the CH_4 concentration and not the isotopic ratio and therefore blur the potential signature of the biological processes. For those runs of the model, the bulk ice concentration has been used.

5. Results

5.1. Barrow

Figure 3 summarizes the results obtained for Barrow from cores recovered on April 3 (blue), May 8 (orange), and June

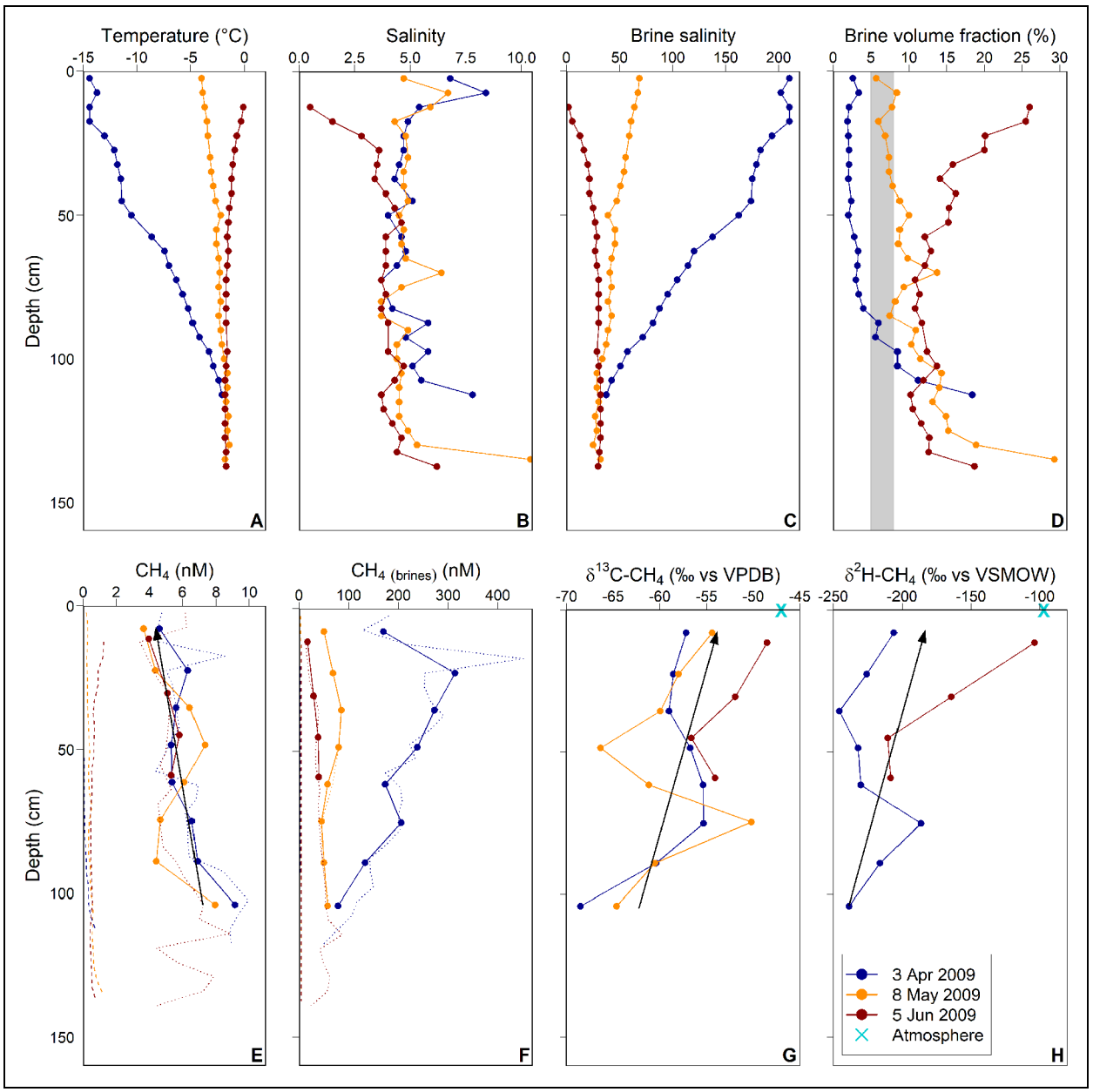

Figure 3. Summary of Barrow (Arctic) sea-ice data. Upper panels show sea-ice physical properties, adapted from Zhou et al. (2014): (A) temperature (°C), (B) salinity, (C) brine salinity, and (D) brine volume fraction (%), in cores collected on April 3 (blue), May 8 (orange), and June 5 (red). The shaded gray area in (D) encompasses the permeability threshold for brines (5%) defined in (Golden et al., 1998) and for gases (7%–8%) defined in Zhou et al. (2013). Lower panels show vertical profiles of (E) CH_4 concentrations (nM) in bulk ice (for readability, we did not add error bars that span $\pm$1.1 nM for the April and June cores and $\pm$1.5 nM for the May core), (F) CH_4 concentrations (nM) in brines, (G) $\delta^{13}C$–CH_4 (‰ vs. Vienna Pee Dee Belemnite) with a standard deviation of $\pm$0.4 ‰, and (H) δ^2H–CH_4 (‰ vs. Vienna Standard Mean Ocean Water) with a standard deviation of <5 ‰, in sea cores collected on April 3 (blue), May 8 (orange), and June 5 (red). Not enough sea ice was available to measure the hydrogen isotopic composition of CH_4 on May 8. The black arrows in (E), (G), and (H) indicate the decreasing trend in CH_4 concentration and increasing trend in $\delta^{13}C$ and δ^2H values from the ice bottom toward the surface. The dashed lines in (E) represent the calculated equilibrium solubility. The dotted lines in (E) and (F) represent the concentrations measured at a 5-cm resolution and averaged to meet the isotopic resolution (solid lines). The light blue cross represents the isotopic composition of the atmosphere. DOI: https://doi.org/10.1525/elementa.2020.00167.f3

5, 2009 (red). CH_4 concentrations in bulk ice ranged between 3.4 and 9.9 nM, with highest values measured at the bottom of the cores (dotted lines, **Figure 3E**). These concentrations, although lower than in the underlying seawater where they ranged between 25.9 and 116.4 nmol L_{SW}^{-1} (Zhou et al., 2014), were still above the maximum equilibrium solubility in bulk sea ice (1.3 nM; dashed lines in **Figure 3E**), indicating that the ice was not

in equilibrium with the atmosphere. This indication is in agreement with the few other studies reporting CH_4 concentration in landfast and/or pack ice in the Arctic (Lorenson and Kvenvolden, 1995; Crabeck et al., 2014; Uhlig et al., 2018). These authors measured concentrations between 5 and 1,260 nmolL_{ice}^{-1} (Lorenson and Kvenvolden, 1995), 1.8 and 12.1 nmol L_{ice}^{-1} (Crabeck et al., 2014), and 53.3 and 144.3 nmol kg_{ice}^{-1} (Uhlig et al., 2018), which, in all cases, was supersaturated compared to the equilibrium solubility in ice. Extreme values in those ranges suggest strong accumulation of CH_4 in sea ice (e.g., as incorporated bubble contribution) and a potential contribution from seafloor CH_4 release.

Among the 3 Arctic sea-ice cores, only the top 95 cm of the April core and the top 45 cm of the May core displayed a brine volume fraction below or at the defined permeability threshold for both brines and gases (5%–8%), respectively, which is represented by a shaded gray area in **Figure 3D**. CH_4 concentrations in brines ranged between 13.2 and 451 nM, with highest values measured in the April core (dotted lines, **Figure 3F**), as lower temperatures lead to a lower porosity and higher brine solute concentration. The $\delta^{13}C$ values (**Figure 3G**) ranged between –68.5 and –48.5 ‰, which is below the $\delta^{13}C$ of atmospheric CH_4 (–47.3 ‰, average monthly value for the period studied, measured at Barrow, National Oceanic and Atmospheric Administration [NOAA]/Earth Research System Laboratories [ESRL] [US] network; White et al., 2018), represented by the light blue cross. These $\delta^{13}C$ values are in the range of previous estimates in Arctic sea ice: –83.4 to –52.1 ‰ along the northern coast of Alaska (Lorenson and Kvenvolden, 1995), between –75 and –36 ‰ in the central Arctic Ocean (Damm et al., 2015), and –62.0 and –54.4 ‰ at Barrow (Uhlig et al., 2018). Our $\delta^{2}H$ signatures are, to the best of our knowledge, the first of their kind and range between –246 and –104 ‰, which is below the $\delta^{2}H$ of atmospheric CH_4 (–97 ‰, average monthly value for the period studied, measured at Barrow, NOAA/ESRL network; White et al., 2016), represented by the light blue cross (**Figure 3H**). A noticeable feature is the decreasing trend in CH_4 bulk concentration associated with an enrichment in ^{13}C and in ^{2}H, from the ice bottom toward the surface (evidenced by the arrows in **Figure 3E**, **G**, and **H**), which either suggests a consumption process or a mixing process with the atmosphere. The variations superimposed on this overall trend are investigated in more detail in the following sections.

5.2. Cape Evans

CH_4 concentrations in sea-ice cores collected at Cape Evans between mid-September and late November 2012 ranged between 1.5 and 7.4 nM (dotted lines, **Figure 4E**), which is again above the maximum equilibrium solubility in bulk sea ice (1.2 nM; dashed lines in **Figure 4E**). Sea-ice brine volume fraction was below or at the permeability threshold for both brines and gases (shaded gray area, **Figure 4D**) down to 140 cm on September 19 and November 7, while it was above the threshold on the full profile from November 30. CH_4 concentrations in brines ranged between 13.1 and 225 nM, with maximum values measured in the top part of the September core (dotted lines, **Figure 4F**). The $\delta^{13}C$ signatures ranged between –46.9 and –13.0 ‰, which, in all cases, is more enriched than the atmospheric isotopic signature (–47.1 ‰, average monthly value for the period studied, measured at the South Pole, NOAA/ESRL network; White et al., 2018), represented by a light blue cross in **Figure 4G**. A significant enrichment of CH_4 in ^{13}C was measured between September 19 and November 7, with the most enriched signatures measured at 33.5 and 111.5 cm depths, respectively (**Figure 4G**). On November 30, $\delta^{13}C$ values were more homogeneous and closer to the atmospheric value. The most depleted $\delta^{2}H$ value was –313 ‰ and the most enriched was –113 ‰ (**Figure 4H**), both lower than the atmospheric $\delta^{2}H$ value (–80 ‰, average monthly value for the September to November months between 2005 and 2008, measured at the South Pole, NOAA/ESRL network; White et al., 2016). In contrast to ^{13}C, CH_4 measured in the 3 cores was more depleted in ^{2}H than the atmospheric value. An overall enrichment of ^{2}H in CH_4 was observed from mid-September to early November. The $\delta^{2}H$ signatures became more depleted again at the end of November, but only reached the maximum values measured in September at some depths. These are the first CH_4 concentration and stable isotope measurements in Antarctic sea ice.

6. Discussion

6.1. Barrow versus Cape Evans: Significant differences in the carbon isotopic composition of CH_4 entrapped in sea ice

The most striking feature of our isotopic data set is the significant difference in the carbon isotopic composition of CH_4 between the two sites, with $\delta^{13}C$ values lower than the atmospheric value at Barrow (–68.5 to –48.5 ‰) and higher at Cape Evans (–46.9 to –13.0 ‰). This difference clearly points toward different sources and sinks. In comparison, $\delta^{2}H$ values cover a similar range at Barrow (–246 to –104 ‰) and Cape Evans (–313 to –113 ‰), all lower than the atmospheric value, indicating that the production/consumption pathways affect carbon and hydrogen isotope values differently.

To compare our sea-ice isotopic data with typical oceanic source signatures, we have reported them on a dual isotope plot and have added the domains defined in Whiticar (1999), together with the global average atmospheric value (**Figure 5**). Most data points fall outside the shaded areas, indicating that the typical microbial and thermogenic sources alone cannot explain the signatures measured in sea ice. In Barrow, most data points fall between the CO_2 reduction and the thermogenic degradation domains, aligning toward the atmospheric value. In Cape Evans, most data points are characterized by $\delta^{13}C$ values that are unlikely to occur from methanogenesis and that are higher than typical thermogenic signatures, with the exception of one data point getting closer to the atmospheric value. In the following sections, we will describe each site individually and investigate the dominant processes controlling the temporal evolution and spatial distribution of CH_4 concentration and isotopic composition in sea ice.

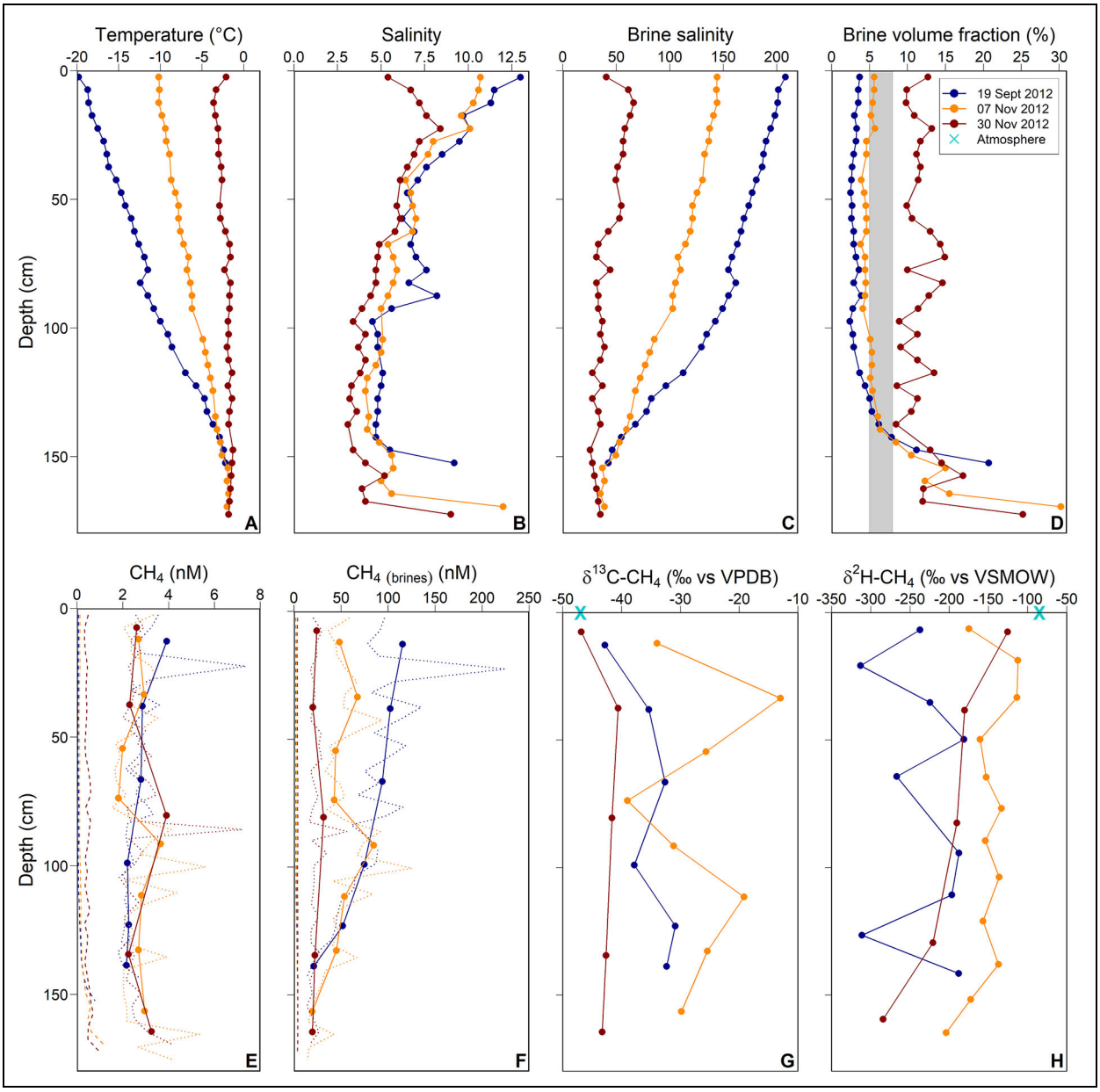

Figure 4. Summary of Cape Evans (Antarctic) sea-ice data. Upper panels show Cape Evans sea-ice physical properties, adapted from Carnat et al. (2014): (A) temperature (°C), (B) salinity, (C) brine salinity, and (D) brine volume fraction (%), in cores collected on September 19 (blue), November 7 (orange), and November 30 (red). The shaded gray area in (D) encompasses the permeability threshold for brines (5%) defined in (Golden et al., 1998) and for gases (7%–8%) defined in Zhou et al. (2013). Lower panels show vertical profiles of (E) CH_4 concentrations (nM) in bulk ice (for readability, we did not add error bars that span $\pm$1.1 nM), (F) CH_4 concentrations (nM) in brines, (G) $\delta^{13}C$–CH_4 (‰ vs. Vienna Pee Dee Belemnite) with a standard deviation of $\pm$0.4 ‰, and (H) $\delta^{2}H$–CH_4 (‰ vs. Vienna Standard Mean Ocean Water) with a standard deviation of <5 ‰, in sea cores from Cape Evans, collected on September 19 (blue), November 7 (orange), and November 30 (red). The dashed lines in (E) represent the calculated equilibrium solubility. The dotted lines in (E) and (F) represent the concentrations measured at a 5-cm resolution and averaged to meet the isotopic resolution (solid lines). The light blue cross represents the isotopic composition of the atmosphere. DOI: https://doi.org/10.1525/elementa.2020.00167.f4

6.2. Barrow

At Barrow, the lowest $\delta^{13}C$ and $\delta^{2}H$ values ($\delta^{13}C = -68.5$ ‰ and $\delta^{2}H = -239$ ‰) were observed at the bottom of the April core (blue curve, **Figure 3G** and **H**). These values are typical of the CO_2 reduction pathway reported for anaerobic methanogenesis in sediments (Whiticar, 1999). Given the shallow depth of the water column and high dissolved CH_4 concentrations in seawater (Zhou et al., 2014), we can reasonably assume that methanogenesis in sediments is the main source of CH_4 in sea ice. This CH_4 can be released by diffusion and possibly ebullition (bubbling) processes, even though no ebullition event was directly observed during the sampling period (Zhou et al., 2014) and found to accumulate in growing sea ice. Methanogenesis has

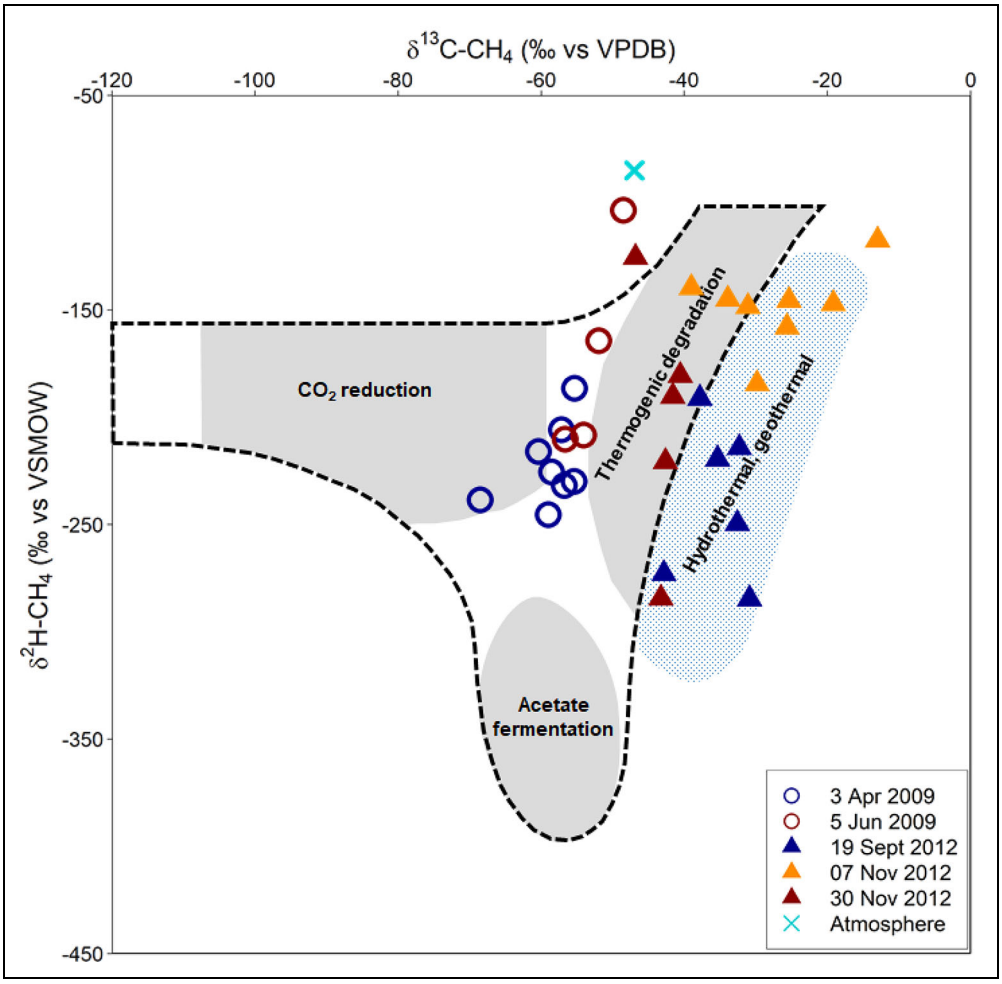

Figure 5. Dual isotope plot with the CH_4 isotopic values measured in Arctic and Antarctic sea ice. The plot includes Arctic (circles) and Antarctic (triangles) sea-ice data collected from cores over the winter-to-spring transition; the typical signatures of the main aquatic CH_4 sources, divided in three domains (gray zones) and defined in Whiticar (1999); and the global average atmospheric composition (light blue cross). The typical isotopic composition of hydrothermal/geothermal CH_4 is indicated by the blue dotted zone (Whiticar, 1999). DOI: https://doi.org/10.1525/elementa.2020.00167.f5

also been found to occur in anoxic microniches in aerobic surface waters (of the subtropical Pacific, Karl and Tilbrook, 1994, and an oligotrophic lake, Grossart et al., 2011), but this type of methanogenesis would likely lead to similar stable isotope values as methanogenesis in sediments.

6.2.1. Temporal variability of CH_4 isotopic composition in sea ice

A boxplot analysis performed on the $\delta^{13}C$ and $\delta^{2}H$ values measured in each core (**Figure 6**) reveals a significantly different CH_4 isotopic composition in the warmer core (June 5, $P \leq .05$). Considering that the April and May cores were below and at the permeability threshold, respectively (blue and orange curves in **Figure 3D**), the opening of the brine system in the June core, induced by warmer temperatures, seems to be responsible for the overall increase in both $\delta^{13}C$ and $\delta^{2}H$ values. With our one-box model, we therefore tested a potential diffusional mixing between atmospheric CH_4 and CH_4 in sea ice at or above the permeability threshold (May and June). As diffusional mixing is driven by a concentration gradient, we chose to work with CH_4 concentrations in brines (**Figure 3F**). In **Figure 7**, we show our isotopic signatures plotted against the logarithm of their brine concentration and draw diffusional mixing lines between the sea-ice samples with the lowest δ values (May: $\delta^{13}C = -66.4$ ‰ and $CH_{4\ (brines)} = 79.6$ nM and June: $\delta_{13}C = -56.6$ ‰, $\delta^{2}H = -210$ ‰ and $CH_{4\ (brines)} = 38.2$ nM) and the atmosphere ($\delta^{13}C = -47.3$ ‰, $\delta^{2}H$ = approximately –97 ‰ and a brine CH_4 concentration of 3.3 nM in May and 4.8 nM in June, corresponding to the equilibrium solubility calculated in brines at the ice surface at those dates). Diffusional mixing lines for both CH_4 stable isotopes (dotted lines, **Figure 7**) do not satisfactorily explain the data distribution, attesting that diffusional mixing with a hypothetical surface brine layer in equilibrium with the atmosphere is not the dominant process explaining the global ^{13}C and ^{2}H enrichment of CH_4 observed between April/May and June. A surface brine layer in equilibrium with the atmosphere is also not observed in our data set but is potentially not resolvable at the vertical resolution of our samples. The

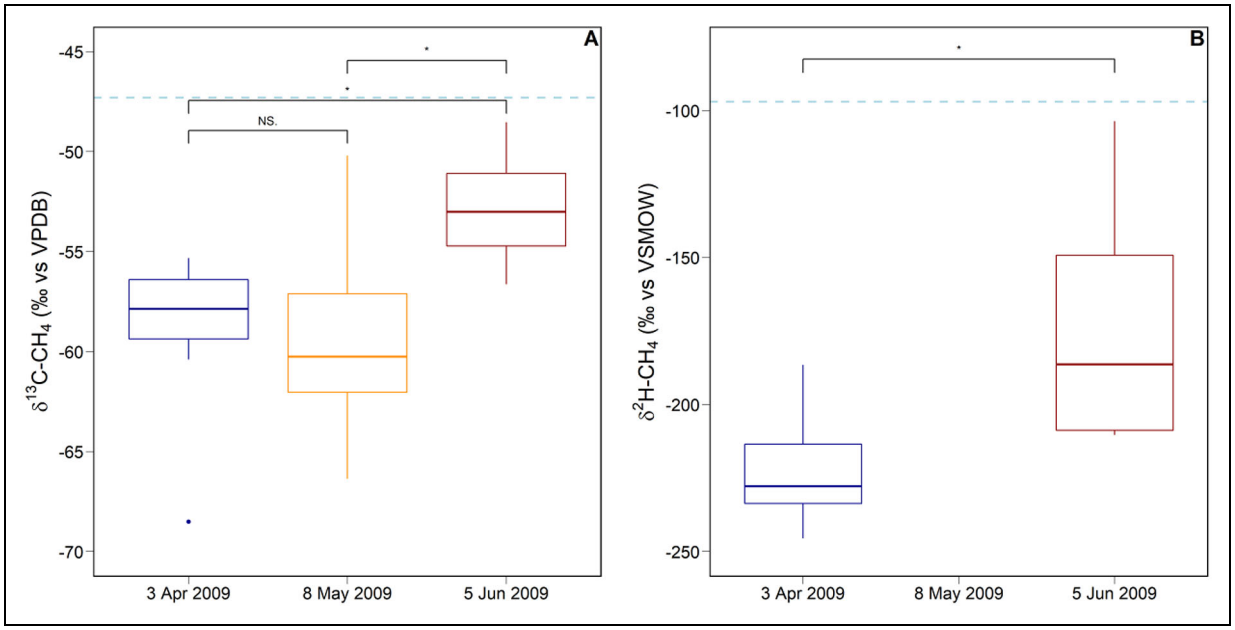

Figure 6. Boxplots of the (A) $\delta^{13}C$ and (B) $\delta^{2}H$ values of CH_4 in Arctic sea ice. The horizontal line represents the median, the box encompasses the 25th and 75th percentiles, and the whiskers correspond to 1.5 × interquartile range. The level of significance is indicated as not significant by NS ($P > .05$) or significant by * ($P \leq .05$ and $> .01$). The isotopic composition of the atmosphere is indicated by the light blue dashed line. Not enough sea ice was available to measure the hydrogen isotopic composition of CH_4 on May 8. DOI: https://doi.org/10.1525/elementa.2020.00167.f6

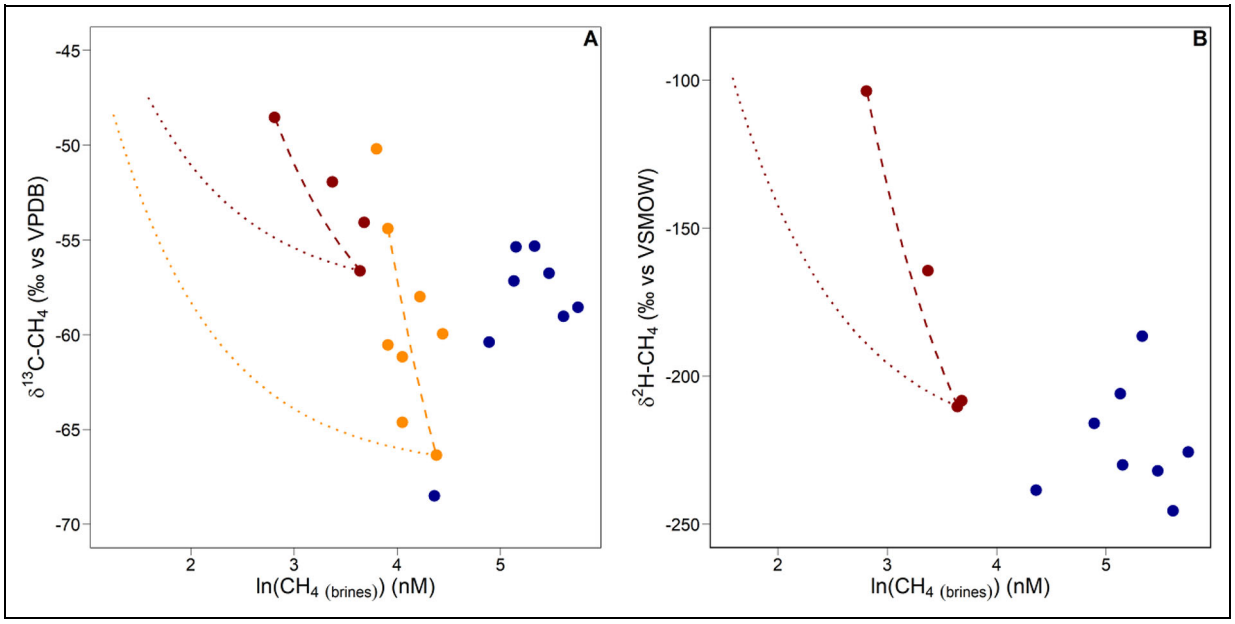

Figure 7. Investigation of the impact of mixing processes in Arctic sea ice. (A) $\delta^{13}C$–CH_4 signatures (‰ vs. Vienna Pee Dee Belemnite) and (B) $\delta^{2}H$–CH_4 signatures (‰ vs. Vienna Standard Mean Ocean Water) as a function of $\ln(CH_{4\,(brines)})$; nM), measured in Barrow sea-ice cores collected on April 3 (blue), May 8 (orange), and June 5 (red). We tested the influence of mixing between CH_4 in brines and atmospheric CH_4 only for the permeable cores (May and June). Dotted lines represent mixing lines between the sea-ice sample with the lowest δ value in each core and a hypothetical surface brine layer in equilibrium with the atmosphere, characterized by $\delta^{13}C = -47.3$ ‰, $\delta^{2}H = -97$ ‰, and a CH_4 concentration in brines corresponding to the equilibrium solubility calculated at the ice surface for those dates. We also tested the influence of brine convection in the permeable cores by drawing mixing lines between the sea-ice sample with the lowest δ value and the upper sea-ice sample (dashed lines). DOI: https://doi.org/10.1525/elementa.2020.00167.f7

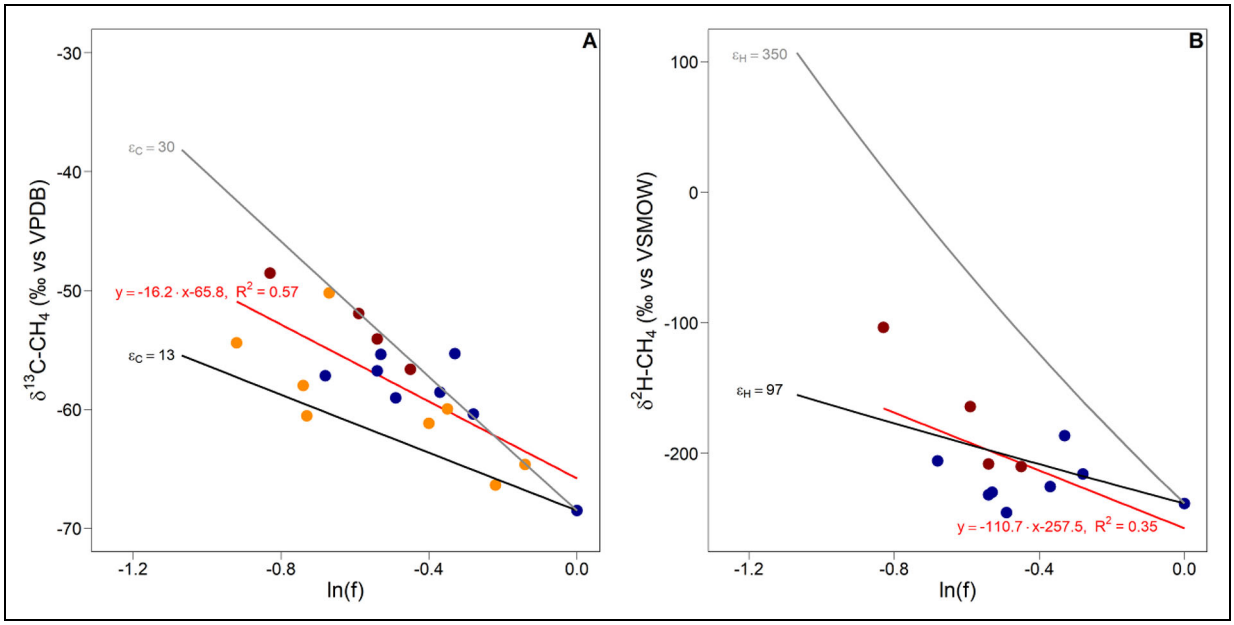

Figure 8. Investigation of the potential for microbial oxidation in Arctic sea ice. (A) δ^{13}C–CH$_4$ signatures (‰ vs. VPDB) and (B) δ^2H–CH$_4$ signatures (‰ vs. Vienna Standard Mean Ocean Water) as a function of ln(f), where f is the remaining fraction of CH$_{4\ ice}$, measured in Barrow sea-ice cores collected on April 3 (blue), May 8 (orange), and June 5 (red) with the regression line (solid red line). The impact of microbial oxidation is investigated by applying the minimum (solid black line) and maximum (solid gray line) values reported in the literature for the carbon and hydrogen isotopic fractionation (ε_C = 13 and 30 ‰ and ε_H = 97 and 350 ‰) to the data point with the highest concentration (CH$_4$ = 9.1 nM, δ^{13}C = –68.5 ‰, and δ^2H = –239 ‰). Note that in these graphic representations, the slope of the linear regressions equals –ε, following the ε definition given in Section 3. DOI: https://doi.org/10.1525/elementa.2020.00167.f8

model calculations confirm that, if present, it would be of limited impact in a pure convective process. However, **Figure 7** shows that if, instead of the calculated equilibrium value, we used the observed surface brine CH$_4$ concentration and isotopic composition, we can fit the permeable ice data sets of May and June well (dashed lines). This result suggests that convective mixing in brine channels as the permeability is restored at the end of the spring (Zhou et al., 2013) could well explain the observed relationship between δ^{13}C/δ^2H and ln(CH$_{4\ (brines)}$) in permeable ice. In that case, potential diffusion processes from deep ice to superficial brine would be fully obliterated by this convective mixing. However, even if convective mixing has been active in the permeable sea ice, a mechanism different from equilibration with the atmosphere is still needed to explain the enriched isotopic values associated with a decrease of CH$_4$ concentrations in the upper part of the Barrow profiles (black lines in **Figure 3**).

6.2.2. Evidence for in situ CH$_4$ oxidation

In the 3 cores, the overall inverse relationship between ice CH$_4$ concentration and both δ^{13}C and δ^2H from the ice bottom toward the surface, with decreasing CH$_4$ concentration associated with an enrichment in both ^{13}C and ^{2}H (black solid lines in **Figure 3E**, **G**, and **H**), is coherent with a consumption (microbial oxidation) process.

The isotopic fractionations for carbon (ε_C) and hydrogen (ε_H) isotopes associated with aerobic microbial CH$_4$ oxidation in aquatic systems typically range between 13 and 30 ‰ and between 97 and 350 ‰, respectively (e.g., Coleman et al., 1981; Kinnaman et al., 2007). If CH$_4$ consumption proceeds with a constant isotope effect and if the reactant CH$_4$ pool is neither replenished nor subject to loss other than consumption, then the isotopic evolution of the residual CH$_4$ is described by Rayleigh fractionation kinetics and the Mariotti et al. (1981) approximation can be used to determine the value of the isotopic fractionation ε (see Section 3). In **Figure 8A**, the best fit to all data (red solid line) gives an ε_C of (mean $\pm$ standard deviation) 16.3 $\pm$ 3.3 ‰ (with ε_C = 16.5 $\pm$ 5.0 ‰, ε_C = 14.3 $\pm$ 4.9 ‰, and ε_C = 20.4 $\pm$ 3.8 ‰, for the April, May, and June cores, respectively), which is in the range of ε_C (13–30 ‰) reported in the literature. In **Figure 8B**, the best fit to the data gives an ε_H = 111 $\pm$ 47 ‰ (with ε_H = 12 $\pm$ 37 ‰ and ε_H = 297 $\pm$ 58 ‰, for the April and June cores, respectively), which is also in the range of ε_H values reported in the literature (97–350 ‰). In **Figure 8A**, we used our simple model approach to investigate how CH$_4$ concentration and carbon isotopic composition would coevolve under the influence of microbial oxidation alone in a closed system, starting from the sample with the highest bulk concentration and the lowest δ^{13}C value (approximately –68.5 ‰) and by applying estimates of ε_C. The two curves encompass most of the data distribution, supporting that oxidation can explain the observed δ^{13}C values. In a similar figure drawn for δ^2H (**Figure 8B**), only part of the data distribution is included between the two oxidation curves, whose positioning is highly

dependent on the end member. The same oxidation curves applied to an end member with a higher concentration and a lower δ^2H value would encompass more data points. Note that for $\delta^{13}C$ (**Figure 8A**), the data points fall closer to the high isotopic fractionation curve ($\varepsilon_C = 30$), whereas for δ^2H (**Figure 8B**), they are closer to the low isotopic fractionation curve ($\varepsilon_H = 97$). The Rayleigh approach, revisited with our one-box model, therefore suggests an important role of CH_4 microbial oxidation, consuming a significant fraction of the CH_4 being accumulated in growing sea ice. The range of observed values adequately fills the bounds imposed by the ε values reported in the literature. The addition of other processes (Table S1), such as continuous production of microbial CH_4 (Figures S1, S2, S4, and S5) or a continuous CH_4 supply from the underlying seawater (Figures S3 and S6), could explain some outliers toward higher fractionation for a given residual bulk concentration.

If methanotrophs were active in the ice interior, we would expect to see a general temporal trend in the CH_4 concentrations (**Figure 3E**), with the vertical profiles shifting toward lower CH_4 bulk ice concentrations over the winter to spring transition, and a temporal shift of the isotopic profiles between April and June toward values more enriched in heavy isotopes, which is not obvious in our data set. However, the potential effect of oxidation is already noticeable on the vertical scale in the core recovered on April 3, which suggests that a partial oxidation signal, at least, was acquired before the first sampling event and therefore also before mixing from brine convection would affect the profile. A closer look to the April 3 CH_4 bulk ice concentration and $\delta^{13}C$–δ^2H signatures shows that most of the gradient is observed within the lower third/quarter of the ice cover (**Figure 3E**, **G**, and **H**; **Figure 6**, blue curves). This observation suggests that although still effective in the upper impermeable layers as time goes by, methanotrophy is particularly active in the bottom ice. Its imprint, however, only becomes apparent when the ice becomes impermeable (ca. 100-cm depth in the April 3 core; **Figure 3D**), as convective mixing in the permeable, growing skeletal layer should homogenize both CH_4 concentrations and isotopic signatures in the brines. In the permeable skeletal layer, temperatures and salinities are close to seawater. These environmental conditions are likely to be more favorable for methanotrophy (Dedysh and Knief, 2018) in comparison to the extreme conditions encountered in the brines of the ice sections above. Despite the ice permeability in the core recovered on May 8 (orange curve, **Figure 3D**), the same overall trend is observed (orange curves, **Figure 3E** and **G**), likely indicating similar processes at stake. With the progressive warming associated with the winter-to-spring transition, the brine system opens and sea ice becomes permeable (**Figure 3A–D**), as evidenced by the decrease in ice CH_4 concentration (**Figure 3E**) between April and May, likely explained by the escape of CH_4, first in the upper 30 cm (from April to May) and then between 30 and 70 cm (from May to June). The opening of the brine system will likely blur the signal imposed by microbial oxidation because of brine convection (see Section 6.2.1). However, the restoration of permeability in warmer ice in May could also have locally enhanced the methanotrophic activity (increasing $\delta^{13}C$, decreasing ice CH_4). Similarly, in the upper layers (0–50 cm), the large improvement of environmental conditions (i.e., warmer temperatures and increased connectivity of the brine channels with new substrate availability) might have been responsible for locally triggering in situ methanotrophy and explain the shift in $\delta^{13}C$ and δ^2H values from May to June (**Figure 3G** and **H**).

Uhlig et al. (2018) estimated the potential of methanotrophy to be low in sea ice sampled at the same location (Utqiagvik, Alaska) and season (April 2016). They measured much higher CH_4 concentrations (53.3–144.3 nmol Kg^{-1}) and a narrower range of $\delta^{13}C$ signatures (approximately –62.0 to –54.4 ‰) than the one we measured here (approximately –68.5 to –48.5 ‰), which indeed indicates a lower influence of bacterial oxidation, and was confirmed by the analyses of the microbial community structure (Uhlig et al., 2018). This difference highlights the spatial and temporal variability of methanotrophy in Arctic sea ice and calls for further studies to identify the conditions favorable to the development of methanotrophs in these extreme environments. This work has demonstrated the occurrence of methanotrophy in sea ice characterized by low CH_4 concentrations. This process might plausibly be masked in a high CH_4 environment, like the one described in Uhlig et al. (2018).

6.3. Cape Evans

At Cape Evans, we expected that CH_4 released from the sediments right below the sampling site would be mostly oxidized before reaching the surface, given the deeper water column (86 m) compared to Barrow (McGinnis et al., 2006; Graves et al., 2015) and that there would be a nearly complete ventilation of the sea ice underlying water with the atmosphere. The CH_4 supersaturation measured in the 3 ice cores associated with $\delta^{13}C$ signatures much higher than in Barrow, and even higher than the atmospheric value (**Figure 4G**), suggests different biogeochemical processes than the one prevailing in Barrow, pointing to advection of CH_4 from a hydrothermal source in shallower waters or to in situ CH_4 production by aerobic microbial pathways, as discussed below.

6.3.1. Temporal variability of CH_4 isotopic composition in sea ice

The boxplot analysis reveals an overall increase in both $\delta^{13}C$ and δ^2H values (**Figure 9**) between September 19 and November 7, where the increase is only significant in the case of hydrogen ($P \leq .001$). This increase is followed by a decrease in the warmer core (November 30), bringing the isotope values closer to the isotopic composition of the atmosphere in the case of carbon, but further away in the case of hydrogen, where the decrease is only significant in the case of carbon ($P \leq .01$). These results illustrate once more the high variability of CH_4 isotopic composition in sea ice. On September 19 and November 7, sea ice was impermeable for gases down to 140 cm (blue and orange curves, **Figure 4D**), discarding a potential

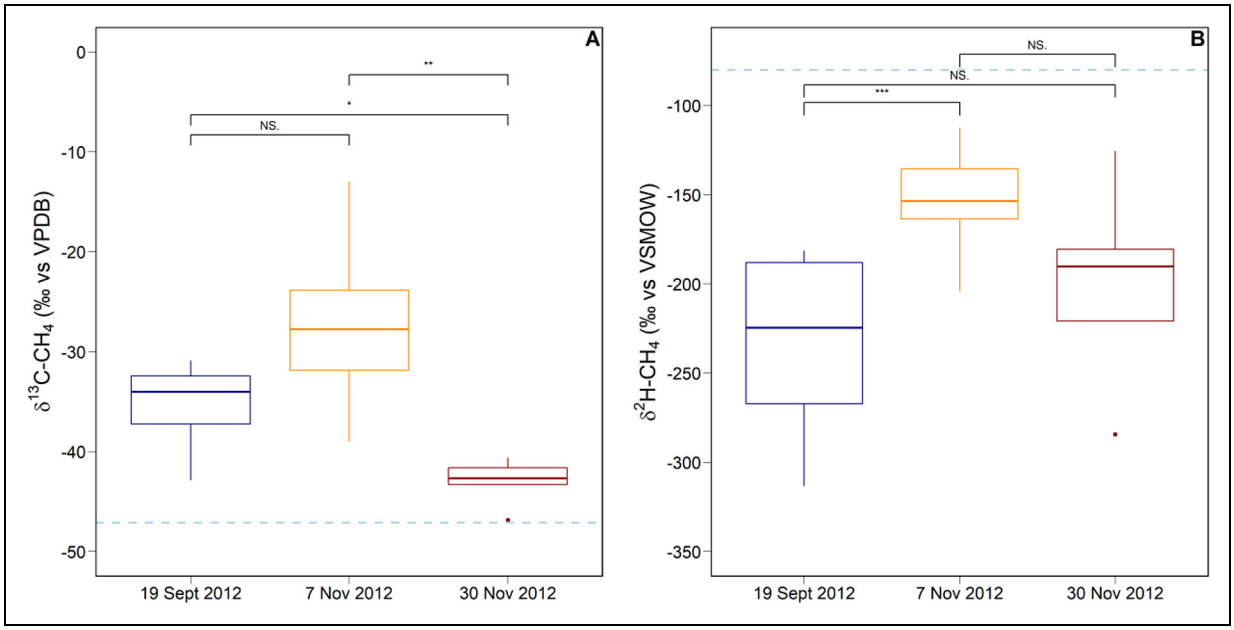

Figure 9. Boxplots of the (A) $\delta^{13}C$ and (B) $\delta^{2}H$ values of CH_4 in Antarctic sea ice. The horizontal line represents the median, the box encompasses the 25th and 75th percentiles, and the whiskers correspond to 1.5 × interquartile range. The level of significance is indicated as not significant by NS ($P > .05$) or significant by * ($P \leq .05$), ** ($P \leq .01$), or *** ($P \leq .001$). The isotopic composition of the atmosphere is indicated by the light blue dashed line. DOI: https://doi.org/10.1525/elementa.2020.00167.f9

atmospheric influence to explain the observed enriched $\delta^{13}C$ signatures (−42.9 to −13.0 ‰; blue and orange curves, **Figure 4G**), which is reinforced by the fact that the atmospheric composition is never that enriched in ^{13}C. The warmest station (November 30) shows a contrasting behavior, with a depth profile fully permeable and brine concentrations homogeneous at 20–25 nM, suggesting potential for homogenization throughout the ice column (red curve, **Figure 4D** and **F**). The $\delta^{13}C$ profile (red curve, **Figure 4G**) is more homogeneous and the surface signature tends toward the atmospheric value (also observed for $\delta^{2}H$ in **Figure 4H**), indicating potential mixing with the atmosphere, even though sea ice is still supersaturated in CH_4. Brine convection supplying dissolved CH_4 from the ventilated underlying mixed layer could also contribute to these homogeneous profiles close to the atmospheric isotopic composition (red curve, **Figure 4D** and **F**).

6.3.2. Contribution from a hydrothermal source

Ross Island is located in an area characterized by an elevated geothermal heat flux and volcanic activity, as evidenced by the presence of Mount Erebus (Risk and Hochstein, 1974; Martos et al., 2017), whose crater is located approximately 20 km from the study site. Given this geological setting, we investigated the potential influence of a hydrothermal origin of the CH_4 entrapped in sea ice at our study site. Even though we expect that hydrothermal CH_4 would be removed by microbial oxidation in the 86-m deep water column so that it cannot accumulate in significant concentration at the ocean surface, the input could be lateral and explain the surprising agreement between our isotopic measurements and the typical $\delta^{13}C$ and $\delta^{2}H$ values reported for hydrothermal CH_4 (Welhan, 1988; Whiticar and Suess, 1990; Labidi et al., 2020), represented by a blue dotted area in **Figure 5**. The isotopic composition of hydrothermal CH_4 was found to vary between hydrothermal fields (Welhan, 1988; Konn et al., 2015) but also temporally at a given site (Proskurowski et al., 2008) and to be further influenced by microbial oxidation in the effluent plume, increasing the $\delta^{13}C$–CH_4 signature to values as high as 11.3 ‰ (Tsunogai et al., 2000), which agrees well with the highest $\delta^{13}C$–CH_4 value measured in our sea-ice cores (orange curve, **Figure 4G**). Unfortunately, we could not find any study documenting the release of hydrothermal fluids in the vicinity of our study site to confirm this hypothesis and recommend further water column sampling in this area to detect their potential presence and characterize their CH_4 concentration and isotopic composition as well as their temporal and spatial occurrence. Although hydrothermal sources may explain the overall ^{13}C-enriched signatures at our study site, the two highest $\delta^{13}C$ values measured in impermeable sea ice on November 7 (and not detected in the previous sampling event on September 19) remain hard to explain at such a small spatial resolution. We therefore investigated, in the following section, additional processes potentially responsible for a temporal evolution within the sea ice cover.

6.3.3. Alternative source: In situ CH_4 production

Most of the variations in isotopic composition at Cape Evans are observed in impermeable sea ice (blue and orange curves, **Figure 4D**, **G**, and **H**). The only processes able to produce and consume CH_4 in a closed system are microbial CH_4 oxidation and production, respectively. An interesting observation is that the CH_4 concentrations

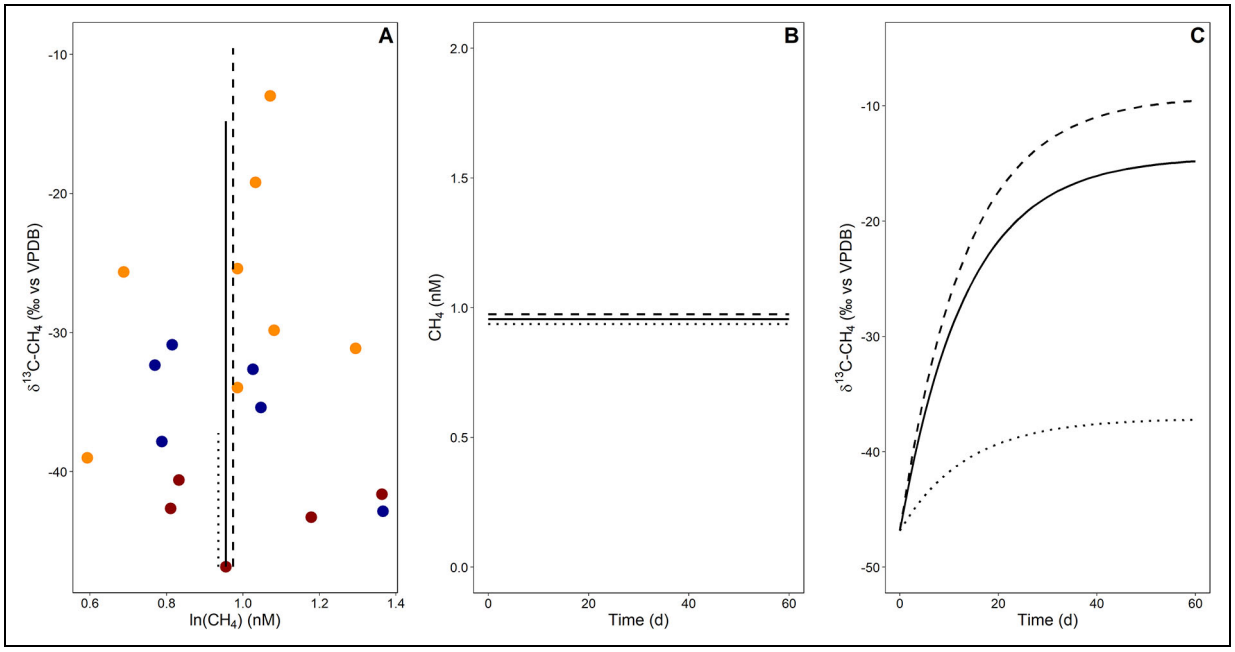

Figure 10. Model runs testing different steady-state conditions between microbial oxidation and production processes. Test conditions: $\varepsilon_C = 30$ and $\delta^{13}C_{MOg} = -66$ ‰ (dotted line), $\varepsilon_C = 30$ and $\delta^{13}C_{MOg} = -44$ ‰ (solid line), and $\varepsilon_C = 16$ and $\delta^{13}C_{MOg} = -25$ ‰ (dashed line). (A) Modeled $\delta^{13}C$ signatures as a function of the logarithm of concentrations, with Cape Evans data points corresponding to September 19 (blue), November 7 (orange), and November 30 (red), (B) modeled CH_4 concentration as a function of time, and (C) modeled $\delta^{13}C$ signatures as a function of time. DOI: https://doi.org/10.1525/elementa.2020.00167.f10

remain relatively constant with time, whereas the isotopic signatures vary over a wide range (**Figure 4E**, **G**, and **H**). The stability of the CH_4 concentration suggests a potential steady state between microbial CH_4 oxidation and in situ production. Assigning similar rates for CH_4 oxidation and production in our one-box model, we tested the impact of a high isotopic fractionation ($\varepsilon_C = 30$) during microbial oxidation of CH_4 produced by CO_2 reduction in anaerobic environments ($\delta^{13}C = -66$ ‰; dotted line, **Figure 10**). This ε_C value is in the higher range of ε_C reported in the literature (Whiticar, 1999; Kinnaman et al., 2007). This combination of parameters cannot explain the observed high CH_4 $\delta^{13}C$ (up to −13.0 ‰) that we measured. Assuming the lower range in the literature for ε_C would have implied even lower $\delta^{13}C$ than observed. We therefore tested different combinations of parameters: A source producing more enriched CH_4 ($\delta^{13}C = -40$ ‰) coupled to a high isotopic fractionation for microbial oxidation ($\varepsilon_C = 30$; solid line, **Figure 10**), and a source producing very enriched CH_4 ($\delta^{13}C = -25$ ‰) coupled to a lower isotopic fractionation for microbial oxidation ($\varepsilon_C = 16$; dashed line, **Figure 7**). With these combinations of parameters, the $\delta^{13}C$ value at steady state reached −10 ‰, which is a good approximation of our most enriched $\delta^{13}C$ signature. The occurrence of CH_4 production despite the aerobic conditions encountered in sea ice (van der Linden et al., 2020), and from a ^{13}C-enriched pool as suggested by the model, points toward a different pathway than the classical anaerobic ones reported in Whiticar (1999; **Figure 5**). Although most of the phytoplankton and microbial species involved in aerobic CH_4 production identified to date (**Table 1**) are not sympagic, *Pseudomonas*, a microbial genus that contains seawater members capable of the C–P lyase pathway, and *Phaeocystis* spp. have been reported in sea ice.

CH_4 production from methylated sulfides (dimethylsulfoniopropionate [DMSP], dimethyl sulfide [DMS], and dimethyl sulfoxide [DMSO]) has recently been suggested (Damm et al., 2010). However, we did not find any clear correlation between our CH_4 concentrations and methylated sulfide (DMSP, DMS, and DMSO) concentrations, nor with particulate organic carbon (POC) or chlorophyll *a*. We could nevertheless identify a possible indirect link with DMSP concentrations. In the same temporal survey (YROSIAE), Carnat et al. (2014) investigated the formation of an unusual local maximum in DMSP concentrations (reaching 372 nM) within the ice interior, in the lower part of several cores sampled successively between September 19 and November 1, 2012 (**Figure 11**). This local maximum was associated with a change in the ice texture, from columnar to platelet ice, which forms from supercooled water rising under the ice shelf and accumulating under the sea-ice cover (Carnat et al., 2014). The authors linked this local maximum to the presence of dinoflagellates that were likely trapped during the platelet ice formation (Carnat et al., 2014). This DMSP peak shrunk to 35.5 nM in the core sampled on November 7, 2012 (Carnat et al., 2014). Our $\delta^{13}C$ measurement in that core at the corresponding depth (100 and 120 cm) reached −19.3 ‰ (orange curve, **Figure 4G**). In the case where the increase in DMSP concentrations, induced by the dinoflagellate bloom, could have fueled CH_4 production by bacteria or algae, this

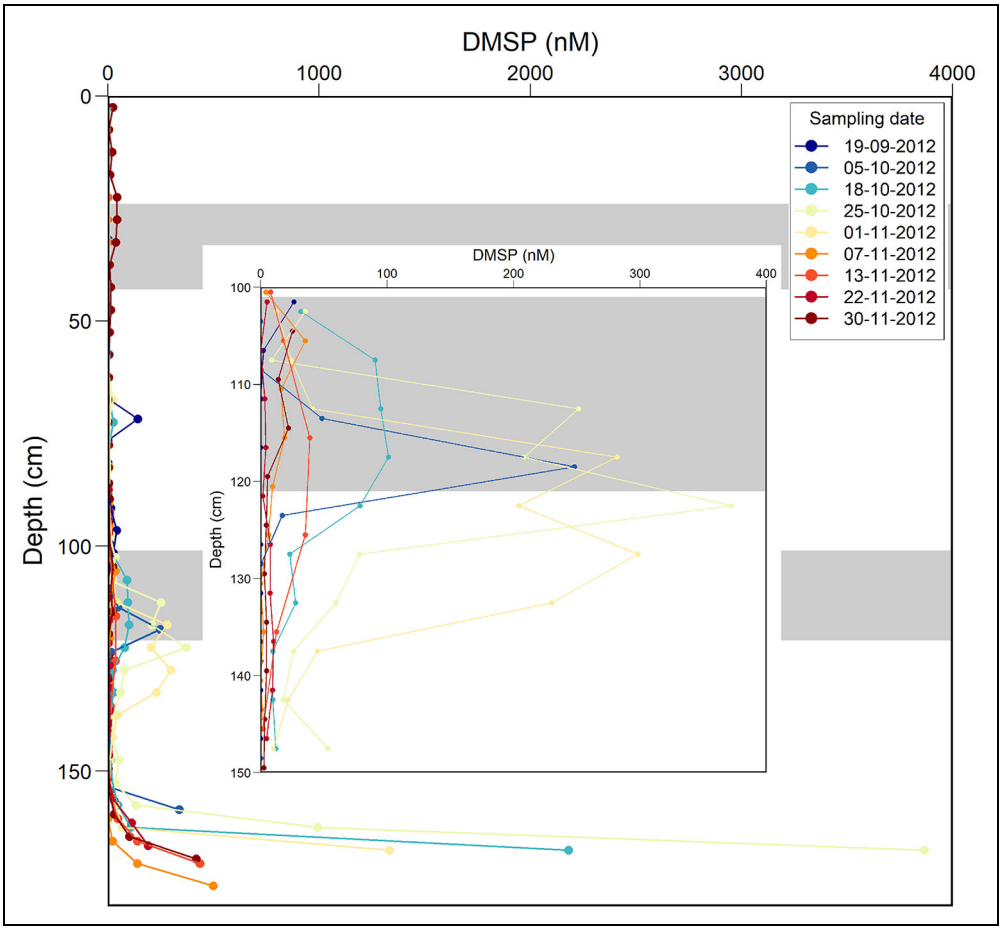

Figure 11. Dimethylsulfoniopropionate concentrations measured in Cape Evans sea ice (Year Round survey of Ocean-Sea Ice-Air Exchanges in Antarctica) adapted from Carnat et al. (2014). Depth profiles are color coded by sampling date (day–month–year). The gray shaded areas correspond to the depths where the most enriched $\delta^{13}C$ signatures were measured in this study. DOI: https://doi.org/10.1525/elementa.2020.00167.f11

unexpectedly enriched value could arise from the methyl group of DMSP. To our knowledge, only one study has been reported on the $\delta^{13}C$ signatures of DMS (−18.6 to −23.4 ‰), a DMSP derivative, obtained from marine sediments (Zhuang et al., 2017). Our value of −19.3 ‰ fits well in this range and might therefore be the result of CH_4 production from DMSP or DMS. Unfortunately, no report of the carbon isotopic fractionation associated with CH_4 production from DMS(P) is available to validate this hypothesis. This pathway cannot be invoked to explain the occurrence of another $\delta^{13}C$ maximum in the same core between 24 and 43 cm (orange curve, **Figure 4G**), given the low DMSP concentrations at that depth throughout the season (**Figure 11**).

CH_4 produced from bacterial degradation of methyl phosphonate (MPn) esters, which are part of the semilabile dissolved organic matter (DOM) pool, is characterized by a $\delta^{13}C$ of −39 ‰ (Repeta et al., 2016). DOM was not measured in these ice cores but can be approximated by the POC concentrations (**Figure 12**) reported in Van der Linden et al. (2020). The vertical profiles of POC reach 2,890 µM at the ice bottom but show little variation in the ice interior, with concentrations lower than 35 µM, except for 2 local peaks, on September 19 at 103.5-cm depth (165 µM) and on October 18 at 47-cm depth (343 µM). The $\delta^{13}C_{POC}$ signatures are confined between −32.2 and −25.2 ‰ in the ice interior, which is the typical range of values reported in the ocean, but increase considerably (between −20.7 and −8.2 ‰) at the bottom of the ice over the course of the season. The 2 local peaks in organic carbon might have fueled bacterial degradation of MPn esters, leading to the production of CH_4 with a $\delta^{13}C$ of −39 ‰ (Repeta et al., 2016). This value agrees with the value of −40 ‰, which we tested for in situ CH_4 production in our one-box model. Thus, a source with this isotopic signature could explain the high $\delta^{13}C$ values we measured, if coupled with microbial oxidation characterized by a high isotopic fractionation ($\varepsilon_C = 30$).

CH_4 was also identified as a by-product of photosynthesis (**Table 1**) in a few marine algae and cyanobacteria. Unfortunately, typical $\delta^{13}C$ signatures associated with this pathway have not yet been reported, preventing us from investigating this scenario in more detail. However, the abundance of cyanobacteria has been found to decrease with decreasing temperature in the Southern Ocean (Wilmotte et al., 2002) and to be very low in sea ice (Koh et al., 2012).

These recent findings indicate that CH_4 biogeochemistry in Antarctic sea ice is more complex than previously

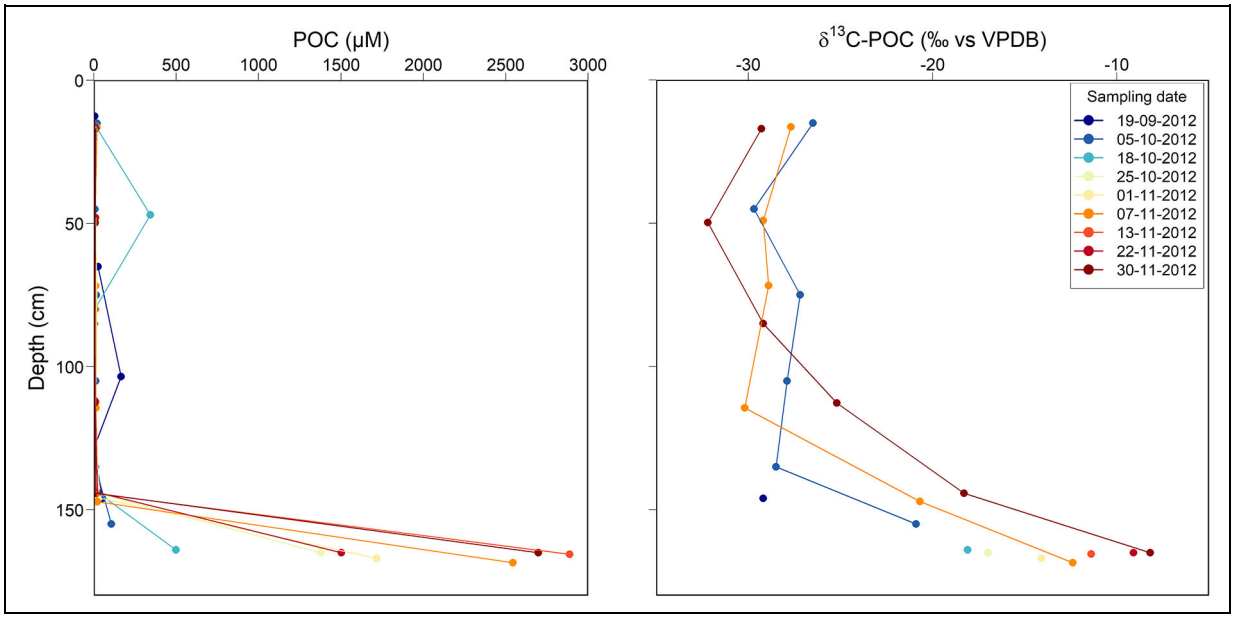

Figure 12. Concentration (left) and $\delta^{13}C$ signatures (right) of particulate organic matter in Antarctic sea ice. Depth profiles are color coded by sampling date (day–month–year). Sea-ice cores were collected at Cape Evans between September 19 and November 30, 2012, in the framework of the Year Round survey of Ocean-Sea Ice-Air Exchanges in Antarctica project. DOI: https://doi.org/10.1525/elementa.2020.00167.f12

thought and that a multitude of biological production pathways exist, of which classical methanogenesis (performed in anoxic sediments or microniches by members of the domain *Archaea*) accounts for a substantial, but nevertheless not exclusive contribution. A characterization of the isotopic fractionation associated with these different pathways would allow us to investigate how they could affect the isotopic signatures found in our ice cores, which deviate from the ones of the traditional aquatic CH_4 sources. Tsunogai et al. (2020) recently proposed a new index (Λ) for hydrogen isotopic discrimination versus carbon isotopic discrimination during CH_4 oxidation, defined as:

$$\Lambda_{(H/C)} = \Delta\delta^2H/\Delta\delta^{13}C, \quad (8)$$

where Δ is the difference between the product and reactant isotopic signature, to refine source tracing in a freshwater lake environment. Unfortunately, the application of this new index in our sea ice environment did not result in coherent relationships.

6.4. δ^2H calling for further investigations

Given the large mass difference in the two hydrogen isotopes (^1H and ^2H), the fractionation effects are larger than for carbon (Whiticar, 1999). The δ^2H–CH_4 signatures are seldomly reported, given the complexity associated with their measurements. The δ^2H signatures are also expected to be more variable because they are affected by the δ^2H of environmental water and by dissolved hydrogen concentrations (Burke, 1993; De Graaf et al., 1996). The δ^2H_{CH4} and $\delta^{13}C_{CH4}$ signatures in the sea ice at Barrow followed similar trends (**Figure 3H**), indicating that the same process, likely microbial oxidation, altered the original sediment-derived CH_4 signature entrapped in the ice. However, at Cape Evans, the picture is more complicated (**Figure 4H**), with all stable hydrogen isotope signatures being more depleted in heavy isotopes than atmospheric CH_4, in contrast to the $\delta^{13}C$ values. If sympagic organisms can produce CH_4 from organic matter trapped or synthesized within sea ice, the hydrogen likely originates from seawater but can be fractionated by numerous biosynthetic pathways (Hayes, 2001). Identification of these pathways is beyond the scope of this study. Our measurements are the first reports of the CH_4 stable hydrogen isotope in sea ice; further investigations are required to understand its dynamics.

7. Conclusion

The dynamics of stable isotopes in CH_4 ($\delta^{13}C$ and δ^2H) in landfast sea ice over the winter-to-spring transition differed strongly between our 2 study sites, Barrow (Utqiagvik, Alaska) and Cape Evans (Antarctica).

At Barrow, the low values of $\delta^{13}C$ and δ^2H, together with the progressive decrease in bulk CH_4 concentration and enrichment in ^{13}C and ^2H from the bottom to the surface of the sea ice, point toward in situ microbial oxidation of microbial CH_4 produced in the shallow underlying sediments with overall larger fractionation in the older sea-ice surface layers. Brine convection events during the spring–summer transition could also be involved in mixing the profiles vertically at the permeable stations. The oxidation likely occurs within the bottom skeletal layer, although it could still evolve at a slower pace in the colder ice above, as the sea-ice cover thickens. "Revived" in situ oxidation in the top of the warming spring sea-ice cover, where environmental conditions are less extreme than in the cold winter brines, would also increase the contribution to the oxidation signature. This potential

mitigation effect of sympagic methanotrophy in reducing the CH_4 flux from the ocean to the atmosphere in shallow shelf areas may be strongly hampered by the ongoing decline of the Arctic sea-ice extent, which would further contribute to the climate-change phenomenon of Arctic amplification (accelerated warming at northern latitudes), given the contrasted greenhouse gas warming potential of CO_2 versus CH_4.

At Cape Evans, we measured a surprisingly wide range of $\delta^{13}C$ values (from −46.9 to −13.0 ‰) and $\delta^{2}H$ values (from −313 to −113 ‰), which are typical of hydrothermal CH_4. The hypothesis of a hydrothermal source is reinforced by the vicinity of the volcano Mount Erebus. We therefore strongly recommend further investigations of potential hydrothermal fluid release at this location. Although hydrothermal activity can be held responsible for the overall isotopic signatures, it hardly explains the temporal contrast observed in the impermeable layers of the sea-ice cover at Cape Evans. We suggest that the most likely candidate for these changes is in situ aerobic CH_4 production. The metabolic pathway(s) involved remain(s) to be identified but likely candidates are DMS(P) degradation and microbial degradation of MPn esters coupled to microbial oxidation. Our study highlights the large temporal and spatial variability in CH_4 concentrations and isotopic composition, which implies variability in the processes influencing CH_4 cycling. Further studies are needed to complement these first measurements of both CH_4 stable isotopes in sea ice. A better characterization of the isotopic fractionation associated with aerobic CH_4 production pathways would help to assess the role of these processes in the sea-ice environment. We also recommend the characterization of the CH_4 isotopic composition in the overlying atmosphere and the underlying water at sea-ice sampling sites to refine our understanding of the processes at stake in sea ice, which clearly plays a role in the CH_4 biogeochemical cycle.

Data accessibility statement

Data used in this study are available in an excel file in supplemental material.

Supplemental files

The supplemental files for this article can be found as follows:

Table S1. Figures S1–S6. Docx.

Dataset. Xlsx.

Acknowledgments

The authors would like to thank Hajo Eicken, and the rest of the sea ice group of the Geophysical Institute of the University of Alaska Fairbanks, Nicolas-Xavier Geilfus, Gauthier Carnat, Tim Papakyriakou, Bernard Heinesch, Michel Yernaux, Thomas Goossens, Noémie Carnat, Frederic Brabant, Rodd Laing Tim Haskell, Brian Staite, Bernard Heinesch, Véronique Schoemann, Thomas Goossens, and the Scott Base crew for their assistance during fieldwork. They also thank Saïda El Amri for her efficient help in laboratory work. They are indebted to Antarctica New Zealand, the Barrow Arctic Science Consortium, and the North Slope Borough for their logistical support.

Funding

This research was supported by the FRS-FNRS (contract 2.4584.09, contract 2.4517.11, PDR T.0268.16 ISOGGAP), Belgian Science Policy (project BIGSOUTH, contract SD/CA/03A and SD/CA/05), the National Science Foundation (project OPP-0632398 [SIZONet]), the University of Alaska Fairbanks, the NCE ArcticNet and National Science and Engineering Research Council, and Antarctica New Zealand (project K131). Jiayun Zhou, Gauthier Carnat, Célia Sapart, and Bruno Delille were or still are PhD students, postdoctoral, and research associate, respectively, of the FRS-FNRS (Fonds National de la Recherche Scientifique, Belgium).

Competing interests

The authors have no competing interests to declare.

Author contributions

Contributed to conception and design: CJ, CJS, JLT.

Contributed to acquisition of data: TH, CJ, CJS, FF, GC, JZ, BD, CvdV, JLT.

Contributed to analysis and interpretation of data: CJ, CJS, FF, JLT.

Drafted and/or revised this article: CJ, CJS, FF, GC, JZ, BD, TR, HN, JLT.

Approved the submitted version for publication: All authors.

References

Aumont, O, Ethé, C, Tagliabue, A, Bopp, L, Gehlen, M. 2015. PISCES-v2: An ocean biogeochemical model for carbon and ecosystem studies. *Geoscientific Model Development* **8**(8): 2465–2513. DOI: http://dx.doi.org/10.5194/gmd-8-2465-2015.

Bižić, M, Klintzsch, T, Ionescu, D, Hindiyeh, MY, Günthel, M, Muro-Pastor, AM, Eckert, W, Urich, T, Keppler, F, Grossart, HP. 2020. Aquatic and terrestrial cyanobacteria produce methane. *Science Advances* **6**(3): 1–10. DOI: http://dx.doi.org/10.1126/sciadv.aax5343.

Brass, M, Röckmann, T. 2010. Continuous-flow isotope ratio mass spectrometry method for carbon and hydrogen isotope measurements on atmospheric methane. *Atmospheric Measurement Techniques* **3**: 1707–1721. DOI: http://dx.doi.org/10.5194/amt-3-1707-2010.

Burke, RA. 1993. Possible influence of hydrogen concentration on microbial methane stable hydrogen isotopic composition. *Chemosphere* **26**(1–4): 55–67. DOI: http://dx.doi.org/10.1016/0045-6535(93)90412-X.

Carnat, G, Zhou, J, Papakyriakou, T, Delille, B, Goossens, T, Haskell, T, Schoemann, V, Fripiat, F, Rintala, JM, Tison, JL. 2014. Physical and biological controls on DMS, P dynamics in ice shelf-influenced fast ice during a winter-spring and a spring-summer transitions. *Journal of Geophysical*

Research: Oceans **119**: 2882–2905. DOI: http://dx.doi.org/10.1002/ 2013JC009381.

Coleman, DD, Risatti, JD, Schoell, M. 1981. Fractionation of carbon and hydrogen isotopes by methane-oxidising bacteria. *Geochimica et Cosmochimica Acta* **45**: 1033–1037. DOI: http://dx.doi.org/10.1016/0016-7037(81)90129-0.

Cox, GFN, Weeks, WF. 1983. Equations for determining the gas and brine volumes in sea ice samples. *Journal of Glaciology* **29**(102): 306–316.

Crabeck, O, Delille, B, Thomas, D, Geilfus, NX, Rysgaard, S, Tison, JL. 2014. CO_2 and CH_4 in sea ice from a subarctic fjord under influence of riverine input. *Biogeosciences* **11**(23): 6525–6538. DOI: http://dx.doi.org/10.5194/bg-11-6525-2014.

Damm, E, Helmke, E, Thoms, S, Schauer, U, Nöthig, E, Bakker, K, Kiene, RP. 2010. Methane production in aerobic oligotrophic surface water in the central Arctic Ocean. *Biogeosciences Discussions* **6**: 10355–10379. DOI: http://dx.doi.org/10.5194/bgd-6-10355-2009.

Damm, E, Kiene, RP, Schwarz, J, Falck, E, Dieckmann, G. 2008. Methane cycling in Arctic shelf water and its relationship with phytoplankton biomass and DMSP. *Marine Chemistry* **109**(1–2): 45–59. DOI: http://dx.doi.org/10.1016/j.marchem.2007.12.003.

Damm, E, Rudels, B, Schauer, U, Mau, S, Dieckmann, G. 2015. Methane excess in Arctic surface water-triggered by sea ice formation and melting. *Scientific Reports* **5**: 16179. DOI: http://dx.doi.org/10.1038/srep16179.

Dean, JF, Middelburg, JJ, Röckmann, T, Aerts, R, Blauw, LG, Egger, M, Jetten, MS, de Jong, AE, Meisel, OH, Rasigraf, O, Slomp, CP. 2018. Methane feedbacks to the global climate system in a warmer world. *Reviews of Geophysics* **56**(1): 207–250. DOI: http://dx.doi.org/10.1002/2017RG000559.

Dedysh, SN, Knief, C. 2018. Diversity and phylogeny of described aerobic methanotrophs, in Kalyuzhnaya, MG, Xing, X-H eds., *Methane biocatalysis: Paving the way to sustainability*. Springer International Publishing: 17–42. DOI: http://dx.doi.org/10.1007/978-3-319-74866-5_2.

De Graaf, W, Wellsbury, P, Parkes, RJ, Cappenberg, TE. 1996. Comparison of acetate turnover in methanogenic and sulfate-reducing sediments by radiolabeling and stable isotope labeling and by use of specific inhibitors: Evidence for isotopic exchange. *Applied and Environmental Microbiology* **62**(3): 772–777. DOI: http://dx.doi.org/10.1128/aem.62.3.772-777.1996.

Delille, B, Vancoppenolle, M, Geilfus, N-X, Tilbrook, B, Lannuzel, D, Schoemann, V, Becquevort, S, Carnat, G, Delille, D, Lancelot, C, Chou, L. 2014. Southern ocean CO_2 sink: The contribution of the sea ice. *Journal of Geophysical Research: Oceans* **119**(9): 6340–6355. DOI: http://dx.doi.org/10.1002/2014JC009941.

Fernández-Méndez, M, Katlein, C, Rabe, B, Nicolaus, M, Peeken, I, Bakker, K, Flores, H, Boetius, A. 2015. Photosynthetic production in the Central Arctic during the record sea-ice minimum in 2012. *Biogeosciences Discussions* **12**(3): 2897–2945. DOI: http://dx.doi.org/10.5194/bgd-12-2897-2015.

Ferré, B, Jansson, PG, Moser, M, Serov, P, Portnov, A, Graves, CA, Panieri, G, Gründger, F, Berndt, C, Lehmann, MF, Niemann, H. 2020. Reduced methane seepage from Arctic sediments during cold bottom-water conditions. *Nature Geoscience* **13**(2): 144–148. DOI: http://dx.doi.org/10.1038/s41561-019-0515-3.

Golden, KM, Ackley, SF, Lytle, VI. 1998. The percolation phase transition in sea ice. *Science* **282**(5397): 2238–2241. DOI: http://dx.doi.org/10.1126/science.282.5397.2238.

Graves, CA, Steinle, L, Rehder, G, Niemann, H, Connelly, DP, Lowry, D, Fisher, RE, Stott, AW, Sahling, H, James, RH. 2015. Fluxes and fate of dissolved methane released at the seafloor at the landward limit of the gas hydrate stability zone offshore western Svalbard. *Journal of Geophysical Research: Oceans* **120**(9): 6185–6201. DOI: http://dx.doi.org/10.1002/2015JC011084.

Grossart, H-P, Frindte, K, Dziallas, C, Eckert, W, Tang, KW. 2011. Microbial methane production in oxygenated water column of an oligotrophic lake. *Proceedings of the National Academy of Sciences* **108**(49): 19657–19661. DOI: http://dx.doi.org/10.1073/pnas.1110716108.

Hartmann, JF, Günthel, M, Klintzsch, T, Kirillin, G, Grossart, HP, Keppler, F, Isenbeck-Schröter, M. 2020. High spatiotemporal dynamics of methane production and emission in oxic surface water. *Environmental Science and Technology* **54**(3): 1451–1463. DOI: http://dx.doi.org/10.1021/acs.est.9b03182.

Hayes, JM. 2001. Fractionation of carbon and hydrogen isotopes in biosynthetic processes. *Stable Isotope Geochemistry* **43**(March): 225–277. DOI: http://dx.doi.org/10.2138/gsrmg.43.1.225.

Hayes, JM. 2004. *An introduction to isotopic calculations*. Woods Hole, MA: Woods Hole Oceanographic Institution, p. 2543.

He, X, Sun, L, Xie, Z, Huang, W, Long, N, Li, Z, Xing, G. 2013. Sea ice in the Arctic Ocean: Role of shielding and consumption of methane. *Atmospheric Environment* **67**: 8–13. DOI: http://dx.doi.org/10.1016/j.atmosenv.2012.10.029.

Holmes, ME, Sansone, FJ, Rust, TM, Popp, BN. 2000. Methane production, consumption, and air-sea exchange in the open ocean: An evaluation based on carbon isotopic ratios. *Global Biogeochemical Cycles* **14**(1): 1–10. DOI: http://dx.doi.org/10.1029/1999GB001209.

Jacques, C, Gkritzalis, T, Tison, J-L, Hartley, T, van der Veen, C, Röckmann, T, Middelburg, JJ, Cattrijsse, A, Egger, M, Dehairs, F, Sapart, CJ. 2020. Carbon and hydrogen isotope signatures of dissolved methane in the Scheldt Estuary. *Estuaries and Coasts*

44(1): 137–146. DOI: http://dx.doi.org/10.1007/s12237-020-00768-3.

Karl, DM, Beversdorf, L, Björkman, KM, Church, MJ, Martinez, A, Delong, EF. 2008. Aerobic production of methane in the sea. *Nature Geoscience* **1**(7): 473–478. DOI: http://dx.doi.org/10.1038/ngeo234.

Karl, DM, Tilbrook, BD. 1994. Production and transport of methane in oceanic particulate organic matter. *Nature* **368**(6473): 732–734. DOI: http://dx.doi.org/10.1038/368732a0.

Kiene, RP. 1991. Production and consumption of methane in aquatic systems, in Rogers, WB, Whitman, JE eds., *Microbial production and consumption of greenhouse gases: Methane, nitrogen oxides and halomethanes*. Washington, DC: American Society for Microbiology: 111–146.

Kinnaman, FS, Valentine, DL, Tyler, SC. 2007. Carbon and hydrogen isotope fractionation associated with the aerobic microbial oxidation of methane, ethane, propane and butane. *Geochimica et Cosmochimica Acta* **71**(2): 271–283. DOI: http://dx.doi.org/10.1016/j.gca.2006.09.007.

Klintzsch, T, Langer, G, Nehrke, G, Wieland, A, Lenhart, K, Keppler, F. 2019. Methane production by three widespread marine phytoplankton species: Release rates, precursor compounds, and potential relevance for the environment. *Biogeosciences* **16**(20): 4129–4144. DOI: http://dx.doi.org/10.5194/bg-16-4129-2019.

Koh, EY, Cowie, ROM, Simpson, AM, O'Toole, R, Ryan, KG. 2012. The origin of cyanobacteria in Antarctic sea ice: Marine or freshwater? *Environmental Microbiology Reports* **4**(5): 479–483. DOI: http://dx.doi.org/10.1111/j.1758-2229.2012.00346.x.

Konn, C, Charlou, JL, Holm, NG, Mousis, O. 2015. The production of methane, hydrogen, and organic compounds in ultramafic-hosted hydrothermal vents of the mid-Atlantic ridge. *Astrobiology* **15**(5): 381–399. DOI: http://dx.doi.org/10.1089/ast.2014.1198.

Kort, EA, Wofsy, SC, Daube, BC, Diao, M, Elkins, JW, Gao, RS, Hintsa, EJ, Hurst, DF, Jimenez, R, Moore, FL, Spackman, JR. 2012. Atmospheric observations of Arctic Ocean methane emissions up to 82° North. *Nature Geoscience* **5**(5): 318–321. DOI: http://dx.doi.org/10.1038/ngeo1452.

Labidi, J, Young, ED, Giunta, T, Kohl, IE, Seewald, J, Tang, H, Lilley, MD, Früh-Green, GL. 2020. Methane thermometry in deep-sea hydrothermal systems: Evidence for re-ordering of doubly-substituted isotopologues during fluid cooling. *Geochimica et Cosmochimica Acta* **288**: 248–261. DOI: http://dx.doi.org/10.1016/j.gca.2020.08.013.

Lenhart, K, Klintzsch, T, Langer, G, Nehrke, G, Bunge, M, Schnell, S, Keppler, F. 2016. Evidence for methane production by the marine algae *Emiliania huxleyi*. *Biogeosciences* **13**(10): 3163–3174. DOI: http://dx.doi.org/10.5194/bg-13-3163-2016.

Lorenson, TD, Kvenvolden, KA. 1995. Methane in coastal sea water, sea ice and bottom sediments, Beaufort Sea, Alaska. U.S. Geological Survey Open-File Report 95-70. U.S. Geological Survey, Menlo Park, CA.

Mariotti, A, Germon, JC, Hubert, P, Kaiser, P, Letolle, R, Tardieux, A, Tardieux, P. 1981. Experimental determination of nitrogen kinetic isotope fractionation: Some principles; illustration for the denitrification and nitrification processes. *Plant and Soil* **62**: 413–430. DOI: http://dx.doi.org/10.1007/BF02374138

Martos, YM, Catalán, M, Jordan, TA, Golynsky, A, Golynsky, D, Eagles, G, Vaughan, DG. 2017. Heat flux distribution of Antarctica unveiled. *Geophysical Research Letters* **44**(22): 11417–11426. DOI: http://dx.doi.org/10.1002/2017GL075609.

McGinnis, DF, Greinert, J, Artemov, Y, Beaubien, SE, Wüest, A. 2006. Fate of rising methane bubbles in stratified waters: How much methane reaches the atmosphere? *Journal of Geophysical Research: Oceans* **111**(9): 1–15. DOI: http://dx.doi.org/10.1029/2005JC003183.

Nisbet, EG, Dlugokencky, EJ, Manning, MR, Lowry, D, Fisher, RE, France, JL, Michel, SE, Miller, JB, White, JW, Vaughn, B, Bousquet, P. 2016. Rising atmospheric methane: 2007–2014 growth and isotopic shift. *Global Biogeochemical Cycles* **30**: 1–15. DOI: http://dx.doi.org/10.1002/2015GB005326. Received.

O'Connor, FM, Boucher, O, Gedney, N, Jones, CD, Folberth, GA, Coppell, R, Friedlingstein, P, Collins, WJ, Chappellaz, J, Ridley, J, Johnson, CE. 2010. Possible role of wetlands, permafrost, and methane hydrates in the methane cycle under future climate change: A review. *Reviews of Geophysics* **48**(4): 1–33. DOI: http://dx.doi.org/10.1029/2010RG000326.

Petrich, C, Eicken, H. 2017. Overview of sea ice growth and properties, in Thomas, DN ed., *Sea ice*. Chichester, UK: John Wiley: 1–41.

Proskurowski, G, Lilley, MD, Olson, EJ. 2008. Stable isotopic evidence in support of active microbial methane cycling in low-temperature diffuse flow vents at 9°50'N East Pacific Rise. *Geochimica et Cosmochimica Acta* **72**(8): 2005–2023. DOI: http://dx.doi.org/10.1016/j.gca.2008.01.025.

Raynaud, D, Delmas, D, Ascencio, JM, Legrand, M. 1983. Gas extraction from polar ice cores: A critical issue for studying the evolution of atmospheric CO_2 and ice-sheet surface elevation. *Annals of Glaciology* **3**: 265–268. DOI: http://dx.doi.org/10.3189/S0260305500002895.

Reeburgh, W. 2007. Oceanic methane biogeochemistry. *American Chemical Society* **107**(2): 486–513. DOI: http://dx.doi.org/10.1021/cr050362v.

Repeta, DJ, Ferrón, S, Sosa, OA, Johnson, CG, Repeta, LD, Acker, M, DeLong, EF, Karl, DM. 2016. Marine methane paradox explained by bacterial degradation of dissolved organic matter. *Nature Geoscience* **9**(12): 884–887. DOI: http://dx.doi.org/10.1038/ngeo2837.

Risk, GF, Hochstein, MP. 1974. Heat flow at arrival heights, Ross Island, Antarctica. *New Zealand*

Journal of Geology and Geophysics **17**(3): 629–644. https://doi.org/10.1080/00288306.1973.10421586.

Sapart, CJ, Martinerie, P, Witrant, E, Chappelaz, J, van der Wal, RSW, Sperlich, P, van der Veen, C, Bernard, S, Sturges, WT, Blunier, T, Schwander, J, Etheridge, D, Röckmann, T. 2013. Can the carbon isotopic composition of methane be reconstructed from multi-site firn air measurements? *Atmospheric Chemistry Physics* **13**(14): 6993–7005. DOI: http://dx.doi.org/10.5194/acp-13-6993-2013

Sapart, CJ, Shakhova, N, Semiletov, I, Jansen, J, Szidat, S, Kosmach, D, Dudarev, O, Veen, CV, Egger, M, Sergienko, V, Salyuk, A. 2017. The origin of methane in the East Siberian Arctic Shelf unraveled with triple isotope analysis. *Biogeosciences Discussions* **14**: 2283–2292. DOI: http://dx.doi.org/10.5194/bg-2016-367.

Sapart, CJ, Van Der Veen, C, Vigano, I, Brass, M, Van De Wal, RSW, Bock, M, Fischer, H, Sowers, T, Buizert, C, Sperlich, P, Blunier, T. 2011. Simultaneous stable isotope analysis of methane and nitrous oxide on ice core samples. *Atmospheric Measurement Techniques* **4**(12): 2607–2618. DOI: http://dx.doi.org/10.5194/amt-4-2607-2011.

Sasakawa, M, Tsunogai, U, Kameyama, S, Nakagawa, F, Nojiri, Y, Tsuda, A. 2008. Carbon isotopic characterization for the origin of excess methane in subsurface seawater. *Journal of Geophysical Research: Oceans* **113**(C3). DOI: http://dx.doi.org/10.1029/2007JC004217.

Schuur, EAG, McGuire, AD, Schädel, C, Grosse, G, Harden, JW, Hayes, DJ, Hugelius, G, Koven, CD, Kuhry, P, Lawrence, DM, Natali, SM. 2015. Climate change and the permafrost carbon feedback. *Nature* **520**(7546): 171–179. DOI: http://dx.doi.org/10.1038/nature14338.

Shakhova, N, Semiletov, I, Leifer, I, Salyuk, A, Rekant, P, Kosmach, D. 2010a. Geochemical and geophysical evidence of methane release over the East Siberian Arctic Shelf. *Journal of Geophysical Research: Oceans* **115**(8): 1–14. DOI: http://dx.doi.org/10.1029/2009JC005602.

Shakhova, N, Semiletov, I, Salyuk, A, Yusupov, V, Kosmach, D, Gustafsson, Ö. 2010b. Extensive methane venting to the atmosphere from sediments of the East Siberian Arctic Shelf. *Science* **445**(June): 1504–1508. DOI: http://dx.doi.org/10.1126/science.1182221.

Tilbrook, BD, Karl, DM. 1995. Methane sources, distributions and sinks from California coastal waters to the oligotrophic North Pacific gyre. *Marine Chemistry* **49**(1): 51–64. DOI: http://dx.doi.org/10.1016/0304-4203(94)00058-L.

Tison, J-L, Delille, B, Papadimitriou, S. 2017. Gases in sea ice, in Thomas, DN ed., *Sea ice.* 3rd Edition. John Wiley: 433–471. DOI: http://dx.doi.org/10.1002/9781118778371.ch18.

Tsunogai, U, Miyoshi, Y, Matsushita, T, Komatsu, DD, Ito, M, Sukigara, C, Nakagawa, F, Maruo, M. 2020. Dual stable isotope characterization of excess methane in oxic waters of a mesotrophic lake. *Limnology and Oceanography* **65**(12): 2937–2952.

Tsunogai, U, Yoshida, N, Ishibashi, J, Gamo, T. 2000. Carbon isotopic distribution of methane in deep-sea hydrothermal plume, Myojin Knoll Caldera, Izu-Bonin arc: Implications for microbial methane oxidation in the oceans and applications to heat flux estimation. *Geochimica et Cosmochimica Acta* **64**(14): 2439–2452. DOI: http://dx.doi.org/10.1016/S0016-7037(00)00374-4.

Uhlig, C, Kirkpatrick, JB, D'Hondt, S, Loose, B. 2018. Methane-oxidizing seawater microbial communities from an Arctic shelf. *Biogeosciences* **15**(11): 3311–3329. DOI: http://dx.doi.org/10.5194/bg-15-3311-2018.

Van der Linden, FC, Tison, JL, Champenois, W, Moreau, S, Carnat, G, Kotovitch, M, Fripiat, F, Deman, F, Roukaerts, A, Dehairs, F, Wauthy, S. 2020. Sea ice CO_2 dynamics across seasons: Impact of processes at the interfaces. *Journal of Geophysical Research: Oceans* **125**(6): e2019JC015807. DOI: http://dx.doi.org/10.1029/2019JC015807.

Welhan, JA. 1988. Origins of methane in hydrothermal systems. *Chemical Geology* **71**(1–3): 183–198. DOI: http://dx.doi.org/10.1016/0009-2541(88)90114-3.

White, JWC, Vaughn, BH, Michel, SE. 2016. University of Colorado, Institute of Arctic and Alpine Research (INSTAAR), stable isotopic composition of atmospheric methane (2H) from the NOAA ESRL Carbon Cycle Cooperative Global Air Sampling Network, 2005–2009, Version: 26 April 2016. Ftp://Aftp.Cmdl.Noaa.Gov/Data/Trace_gases/Ch4h2/Flask/.

White, JWC, Vaughn, BH, Michel, SE. 2018. University of Colorado, Institute of Arctic and Alpine Research (INSTAAR), stable isotopic composition of atmospheric methane (13C) from the NOAA ESRL Carbon Cycle Cooperative Global Air Sampling Network, 1998–2017, Version: 24 September 2018. Ftp://Aftp.Cmdl.Noaa.Gov/Data/Trace_gases/Ch4c13/Flask/.

Whiticar, MJ. 1999. Carbon and hydrogen isotope systematics of bacterial formation and oxidation of methane. *Chemical Geology* **161**: 291–314. DOI: http://dx.doi.org/10.1016/S0009-2541(99)00092-3.

Whiticar, MJ, Suess, E. 1990. Hydrothermal hydrocarbon gases in the sediments of the King George Basin, Bransfield Strait, Antarctica. *Applied Geochemistry* **5**: 135–147.

Wilmotte, A, Demonceau, C, Goffart, A, Hecq, JH, Demoulin, V, Crossley, AC. 2002. Molecular and pigment studies of the picophytoplankton in a region of the Southern Ocean (42–54°S, 141–144°E) in March 1998. *Deep-Sea Research Part II: Topical Studies in Oceanography* **49**(16): 3351–3363. DOI: http://dx.doi.org/10.1016/S0967-0645(02)00087-5.

Zhou, J, Delille, B, Eicken, H, Vancoppenolle, M, Brabant, F, Carnat, G, Geilfus, NX, Papakyriakou, T,

Heinesch, B, Tison, JL. 2013. Physical and biogeochemical properties in landfast Sea ice (Barrow, Alaska): Insights on brine and gas dynamics across seasons. *Journal of Geophysical Research: Oceans* **118**(6): 3172–3189. DOI: http://dx.doi.org/10.1002/jgrc.20232.

Zhou, J, Tison, J-L, Carnat, G, Geilfus, N-X, Delille, B. 2014. Physical controls on the storage of methane in landfast sea ice. *The Cryosphere* **8**(3): 1019–1029. DOI: http://dx.doi.org/10.5194/tc-8-1019-2014.

Zhuang, GC, Lin, YS, Bowles, MW, Heuer, VB, Lever, MA, Elvert, M, Hinrichs, KU. 2017. Distribution and isotopic composition of trimethylamine, dimethylsulfide and dimethylsulfoniopropionate in marine sediments. *Marine Chemistry* **196**: 35–46. DOI: http://dx.doi.org/10.1016/j.marchem.2017.07.007.

How to cite this article: Jacques, C, Sapart, CJ, Fripiat, F, Carnat, G, Zhou, J, Delille, B, Röckmann, T, van der Veen, C, Niemann, H, Haskell, T, Tison, J-L. 2021. Sources and sinks of methane in sea ice: Insights from stable isotopes. *Elementa: Science of the Anthropocene* 9(1). DOI: https://doi.org/10.1525/elementa.2020.00167

Domain Editor-in-Chief: Jody W. Deming, University of Washington, Seattle, WA, USA

Associate Editor: Christine Michel, Department of Fisheries and Oceans, Canada, Freshwater Institute, Winnipeg, Manitoba, Canada

Knowledge Domain: Ocean Science

Part of an Elementa Special Feature: Insights into Biogeochemical Exchange Processes at Sea Ice Interfaces (BEPSII-2)

Published: October 27, 2021 **Accepted:** September 2, 2021 **Submitted:** November 6, 2020

ELEMENTA Science of the Anthropocene

Elem Sci Anth is a peer-reviewed open access journal published by University of California Press.

OPEN ACCESS